

RESEARCH PAPER



Novel pyrrolopyrimidine derivatives: design, synthesis, molecular docking, molecular simulations and biological evaluations as antioxidant and anti-inflammatory agents

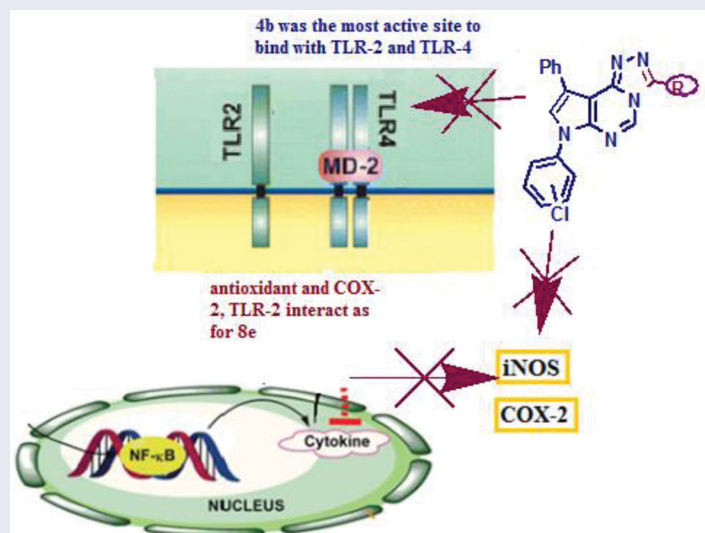
Amira I. Sayed^a, Yara E. Mansour^a, Mohamed A. Ali^b, Omnia Aly^c, Zainab M. Khoder^{a,d}, Ahmed M. Said^{a,d,e}, Samar S. Fatahala^a and Rania H. Abd El-Hameed^a

^aPharmaceutical Organic Chemistry Department, Faculty of Pharmacy, Helwan University, Cairo, Egypt; ^bBiochemistry Department, Faculty of Agriculture, Cairo University, Cairo, Egypt; ^cMedical Biochemistry Department, National Research Centre, Dokki, Egypt; ^dDepartment of Chemistry, The State University of New York, Buffalo, NY, USA; ^eAthenex Inc., Buffalo, NY, USA

ABSTRACT

Current medical approaches to control the Covid-19 pandemic are either to directly target the SARS-CoV-2 via innovate a defined drug and a safe vaccine or indirectly target the medical complications of the virus. One of the indirect strategies for fighting this virus has been mainly dependent on using anti-inflammatory drugs to control cytokines storm responsible for severe health complications. We revealed the discovery of novel fused pyrrolopyrimidine derivatives as promising antioxidant and anti-inflammatory agents. The newly synthesised compounds were evaluated for their in vitro anti-inflammatory activity using RAW264.7 cells after stimulation with lipopolysaccharides (LPS). The results revealed that **3a**, **4b**, and **8e** were the most potent analogues. Molecular docking and simulations of these compounds against COX-2, TLR-2 and TLR-4 respectively was performed. The former results were in line with the biological data and proved that **3a**, **4b** and **8e** have potential antioxidant and anti-inflammatory effects.

GRAPHICAL ABSTRACT



ARTICLE HISTORY

Received 10 March 2022
Revised 1 June 2022
Accepted 10 June 2022



KEYWORDS

Pyrrolopyrimidines; cytotoxicity; macrophages-RAW 267.4; DPPH; molecular docking

Introduction

Toll-like receptors (TLRs) are a family of pattern recognition receptors (PRRs) that form the cornerstone of the innate sensor, and also shape and bridge innate and adaptive immune responses. They can recognise both the external pathogen-associated molecular patterns (PAMPs) and the internal damage-associated molecular patterns (DAMPs) are the most potent inducers of the inflammatory responses^{1,2}. Recent studies emphasised that above

50% of the death toll worldwide is mainly due to chronic inflammatory diseases. TLR activation stimulates signalling cascades by the host as a defence mechanism against invaders and to repair the damaged tissue, leading to the release of various inflammatory cytokines and immune modulators^{3,4}. However, excessive TLR activation disrupts the immune homeostasis by sustained pro-inflammatory cytokines and chemokine production and consequently contributes to the development and progression of many

CONTACT Samar S. Fatahala  samar_saleh@pharm.helwan.edu.eg  Pharmaceutical Organic Chemistry Department, Faculty of Pharmacy, Helwan University, Cairo 11795, Egypt

© 2022 The Author(s). Published by Informa UK Limited, trading as Taylor & Francis Group.

This is an Open Access article distributed under the terms of the Creative Commons Attribution License (<http://creativecommons.org/licenses/by/4.0/>), which permits unrestricted use, distribution, and reproduction in any medium, provided the original work is properly cited.

diseases, such as autoimmune diseases including lupus erythematosus and rheumatoid arthritis, cancer, sepsis, Alzheimer's disease, and type 1 diabetes^{5–11}.

TLRs serve as sensors of conserved components of microorganisms, such as, SARS-CoV-2, which triggers inflammatory signalling cascades, downstream transcription factors and induces the production of pro-inflammatory cytokines and over production of nitric oxide (NO) and reactive oxygen species (ROS)¹². Cytokine storm is the major reason for the high mortality rates of COVID-19 due to the induction of excessive and prolonged high concentrations of pro-inflammatory cytokine/chemokine, besides the multiple organ dysfunction, which leads to physiological deterioration and death^{13–15}. Reactive oxygen species (ROS) and reactive nitrogen species (RNS) are recognised for their dual role as both deleterious and beneficial species. Oxidative stress is the overproduction of ROS/RNS, viewed as an imbalance between the production of reactive species and their elimination by protective mechanisms, which leads to chronic inflammation and results in damage to cell structures, including lipids and membranes, proteins, and DNA, inhibiting their normal function¹⁶.

TLRs are classified into two subgroups such as cell membrane TLRs (TLR1, TLR2, TLR4, TLR5, TLR6, and TLR10) that are expressed on the cell surface and intracellular TLRs or nucleic acids sensors (TLR3, TLR7, TLR8, and TLR9) that are localised to the endoplasmic reticulum (ER), endosomes, and lysosomes^{17–19}. The expression of these receptors not only on all innate immune cells such as macrophages, neutrophils, dendritic cells (DCs), basophils, natural killer (NK) cells, mast cells, and eosinophils but they are also present in a variety of cell types, including fibroblasts, endothelial cells, epithelial cells, and placental tissue. Moreover, the regulation for their locations are mainly in response to the recognised PAMP

(recognizes invaders) and DAMPs (endogenous damage recognition)^{20,21}. Structurally TLRs located on cell membranes possess an extracellular domain containing leucine-rich repeats that recognise distinct PAMPs and a toll-interleukin1 (IL-1) receptor (TIR) domain are required for downstream signalling. TLR4, the first toll protein homolog discovered in humans, was shown to induce the expression of genes involved in inflammatory responses. TLR2 and TLR4 have gained immense importance due to being among the cell surface TLRs^{22,23}.

TLR4 is mainly activated by lipopolysaccharide (LPS), lipooligosaccharide (LOS), and lipid A from Gram-negative bacteria generally called endotoxin. The recognition through accessory molecules such as LPS-binding protein (LBP), the cluster of differentiation 14 (CD14), and myeloid differentiation factor 2 (MD2), but, heterodimerization of TLR2 with either TLR1 or TLR6 is essential for recognising microbial cell wall component diacylated and triacetylated lipopeptide^{24,25}.

In response to TLR engagement, rapid induction of pro-inflammatory signalling starts with activation of the innate immune signalling cascade *via* both myeloid differentiation primary response protein 88 (MyD88)-dependent and MyD88-independent pathways. The MyD88-dependent signalling pathway is responsible for the early phase activation of transcription nuclear factor- κ B (NF- κ B) and mitogen-activated protein kinases (MAPKs); these events result in inducing the gene expression of pro-inflammatory cytokines [tumour necrosis factor (TNF)- α , interleukin (IL)-1 β and IL-6], inflammatory mediators [reactive oxygen species (ROS), nitric oxide (NO), and prostaglandin E2 (PGE2)], which contribute to the progression of several inflammatory diseases^{26–29}, as revealed in (Figure 1).

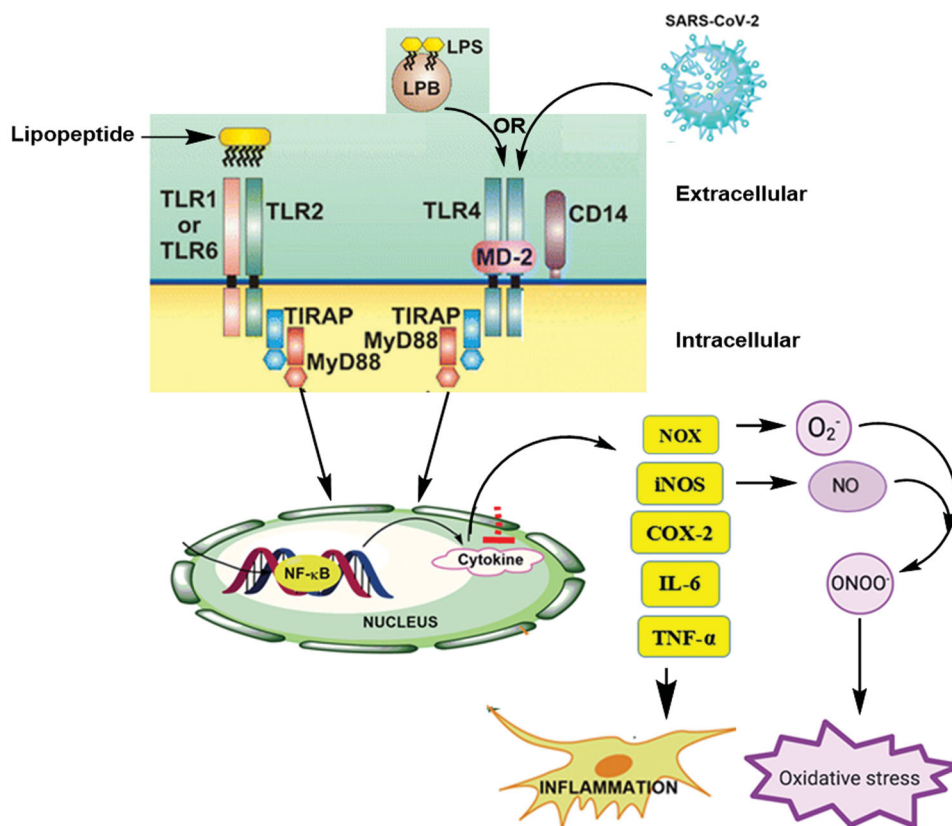


Figure 1. TLRs signalling activates transcription nuclear factor κ B (NF- κ B) in the nucleus and promotes the increase in the expression of the pro-oxidant enzymes NADPH-oxidase (NOX) and inducible nitric oxide synthase (iNOS), moreover pro-inflammatory cytokines tumour necrosis factor (TNF)- α , interleukin (IL)-1 β , IL-6, and IL-12).

The activity of oxidant enzymes such as NADPH-oxidase (NOX), inducible NO synthase (iNOS) and cyclooxygenase-2 (COX-2); the enzymes involved in the production of ROS NO, and PGE₂; is positively correlated with the expression of pro-inflammatory cytokines^{30,31}. The suppression of inflammation through the discovery of a novel antagonists/inhibitors regulating TLR2/4 activity appears as a therapeutic strategy in the treatment of chronic inflammatory diseases³².

Inspired by the above-mentioned discoveries, and as continued for our effort in field for preparation of pyrroles as anti-inflammatory compounds^{33–36}, some pyrrolopyrimidines **3–8** (namely, pyrrolotriazolopyrimidines and hydrazones derivatives) were synthesised, docked and screened for their antioxidant and anti-inflammatory activities *via* TLRs (TLR2 and TLR4) inhibition. Additionally, molecular dynamic simulations (MDS) were conducted for 100 ns using GROMACS 2.1.1 software using the docking coordinates of COX-2 and TLR-4 bound to compounds **4b** and **8e**, respectively. The MD simulation was performed to provide insights into precise estimation of the binding strength of a docked complex of COX-2 and TLR-4 bound to compounds **4b** and **8e**.

Materials and methods

Chemistry

Synthesis of lead compounds

All commercial chemicals used as starting materials and reagents in this study were purchased from Merck (Darmstadt, Germany) and were of reagent grade. All melting points were uncorrected and measured using Electro-thermal IA 9100 apparatus (Shimadzu, Japan); IR spectra were recorded as potassium bromide pellets on a Perkin-Elmer 1650 spectrophotometer (USA), Faculty of Science, Cairo University, Cairo, Egypt. ¹H-NMR spectra were determined on a Varian Mercury (300 MHz) spectrometer (Varian UK) and chemical shifts were expressed as ppm against TMS as internal reference (The Main Chemical Warfare Laboratories, Almaza, Cairo, Egypt). Mass spectrum was carried out on Direct Inlet part to mass analyser on 70 eV (ISQ 7000, single quadrupole, GC-MS, Thermo Scientific, Massachusetts, USA) at the Regional Centre for Mycology and Biotechnology (RCMB), Al-Azhar University, Nasr City, Cairo, confirming the purity of the compounds as well as explore the characteristic fragmentation using EI mode and the expected [M. Wt]. Microanalyses were operated using Vario, Elementar apparatus (Shimadzu, Japan), Organic Microanalysis Unit, Faculty of Science, Cairo University, Cairo, Egypt. Column Chromatography was performed on (Merck) Silica gel 60 (particle size 0.06–0.20 mm). All the listed compounds are new except compounds 1a,b were previously reported^{37,38}.

General procedure for the synthesis of compounds 2(a–b)

A mixture of 4-chloro pyrrolopyrimidine **1(a–b)** (0.01 mol), hydrazine hydrate (0.01 mol) was heated under reflux in absolute ethanol for 8 h, cooled, poured onto ice water to give precipitates which were filtered off, dried and recrystallized from methanol to give compounds **2(a–b)**.

(7–(3-Chlorophenyl)-5-phenyl-7H-pyrrolo[2,3-d]pyrimidin-4-yl)-hydrazine (2a)

Yield: 72%; m.p.: 204–206 °C; IR (KBr) ν (cm⁻¹): 3413, 3320 (NH₂), 3287 (N–H), 1533 (C=N); MS (EI) m/z : 337 (M + 2, 11.2%), 335 (M⁺,

34%), ¹H NMR (DMSO-d₆, 300 MHz) δ (ppm): 5.19 (br s, 2H, NH₂, D₂O exchangeable), 6.80–8.12 (m, 12H, Ar-H + NH, D₂O exchangeable); Anal. Calcd for C₁₈H₁₄ClN₅ (335.09): C, 64.48; H, 4.18; N, 20.90%. Found: C, 64.19; H, 4.12; N, 20.69%.

(7–(4-Chlorophenyl)-5-phenyl-7H-pyrrolo[2,3-d]pyrimidin-4-yl)-hydrazine (2b)

Yield: 80%; m.p.: 217–219 °C; IR (KBr) ν (cm⁻¹): 3420, 3374 (NH₂), 3233 (N–H), 1560 (C=N); MS (EI) m/z : 337 (M + 2, 18.7%), 335 (M⁺, 55.2%), ¹H NMR (DMSO-d₆, 300 MHz) δ (ppm): 5.26 (br s, 2H, NH₂, D₂O exchangeable), 6.78–8.09 (m, 12H, Ar-H + NH, D₂O exchangeable); Anal. Calcd for C₁₈H₁₄ClN₅ (335.09): C, 64.48; H, 4.18; N, 20.90%. Found: C, 64.22; H, 4.36; N, 20.71%.

General procedure for the synthesis of compounds 3(a–b)

The appropriate hydrazine **2(a–b)** (0.01 mol) was heated under reflux for 8 h in formic acid (20 mL, 85%), cooled, poured onto ice water to give a precipitate which was filtered off, dried and recrystallized from ethanol to yield compounds **3(a–b)**.

7–(3-Chlorophenyl)-9-phenyl-7H-pyrrolo[3,2-e][1,2,4]triazolo[4,3-c]pyrimidine (3a)

Yield: 77%; m.p.: 176–178 °C; IR (KBr) ν (cm⁻¹): 1603 (C=N); MS (EI) m/z : 347 (M + 2, 8.92%), 345 (M⁺, 27.47%), ¹H NMR (DMSO-d₆, 300 MHz) δ (ppm): 6.51–7.87 (m, 11H, Ar-H), 8.24 (s, 1H, C5-H); ¹³C-NMR (DMSO, 75 MHz) δ (ppm): 95.8, 101.72, 105.36, 109.44, 111.3, 118.32, 119.27, 121.34, 122.65, 129.43, 129.88, 139.27, 144.45, 147.8, 156.3, 160.9, 162.3 (SP² carbon atoms); Anal. Calcd for C₁₉H₁₂ClN₅ (345.07): C, 65.09; H, 3.48; N, 20.29%. Found: C, 65.03; H, 3.42; N, 20.21%.

7–(4-Chlorophenyl)-9-phenyl-7H-pyrrolo[3,2-e][1,2,4]triazolo[4,3-c]pyrimidine (3b)

Yield: 85%; m.p.: 190–192 °C; IR (KBr) ν (cm⁻¹): 1614 (C=N); MS (EI) m/z : 349 (M + 2, 9.79%), 347 (M⁺, 29.14%), ¹H NMR (DMSO-d₆, 300 MHz) δ (ppm): 6.26–7.84 (m, 11H, Ar-H), 7.87 (s, 1H, C5-H); Anal. Calcd for C₁₉H₁₂ClN₅ (345.07): C, 65.09; H, 3.48; N, 20.29%. Found: C, 65.25; H, 3.27; N, 20.24%.

General procedure for the synthesis of compounds 4(a–b)

A mixture of the appropriate hydrazine **2(a–b)** (0.01 mol) and carbon disulphide (0.01 mol) was heated under reflux for 3 h in absolute ethanol (30 mL), cooled, poured onto ice water to give a precipitate which was filtered off, dried and recrystallized from ethanol to yield compounds **4(a–b)**.

7–(3-Chlorophenyl)-9-phenyl-7H-pyrrolo[3,2-e][1,2,4]triazolo[4,3-c]pyrimidin-3-thione (4a)

Yield: 57%; m.p.: 193–195 °C; IR (KBr) ν (cm⁻¹): 3322 (N–H), 1567 (C=N), 1487, 1258, 1020, 812 (C=S); MS (EI) m/z : 379 (M + 2, 11.06%), 377 (M⁺, 31.7%), ¹H NMR (DMSO-d₆, 300 MHz) δ (ppm): 6.93–8.30 (m, 11H, Ar-H), 10.23 (br s, 1H, NH, D₂O exchangeable); Anal. Calcd for C₁₉H₁₂ClN₅S (377.06): C, 60.48; H, 3.18; N, 18.57%. Found: C, 60.45; H, 3.27; N, 18.73%.

7-(4-Chlorophenyl)-9-phenyl-7H-pyrrolo[3,2-e][1,2,4]triazolo[4,3-c]pyrimidin-3-thione (4b)

Yield: 60%; m.p.: 187–189 °C; IR (KBr) ν (cm⁻¹): 3413 (N–H), 1609 (C=N), 1483, 1259, 1016, 800 (C=S); MS (EI) m/z : 379 (M + 2, 19.4%), 377 (M⁺, 58.6%), ¹H NMR (DMSO-d₆, 300 MHz) δ (ppm): 6.93–8.26 (m, 11H, Ar-H), 11.83 (br s, 1H, NH, D₂O exchangeable); Anal. Calcd for C₁₉H₁₂ClN₅S (377.06): C, 60.48; H, 3.18; N, 18.57%. Found: C, 60.17; H, 3.11; N, 18.50%.

General procedure for the synthesis of compounds 5(a–b)

The appropriate hydrazine **2(a–b)** (0.01 mol) was heated under reflux for 5 h in acetic anhydride (30 mL), cooled, poured onto ice water and neutralised with ammonia to give a precipitate which was filtered off, dried and recrystallized from ethanol to yield compounds **5(a–b)**.

7-(3-Chlorophenyl)-3-methyl-9-phenyl-7H-pyrrolo[3,2-e][1,2,4]triazolo[4,3-c]pyrimidine (5a)

Yield: 59%; m.p.: 227–229 °C; IR (KBr) ν (cm⁻¹): 1598 (C=N); MS (EI) m/z : 361 (M + 2, 15.7%), 359 (M⁺, 45.03%), ¹H NMR (DMSO-d₆, 300 MHz) δ (ppm): 2.10 (s, 3H, C3-CH₃), 6.48–7.56 (m, 10H, Ar-H), 8.21 (s, 1H, C5-H); ¹³C-NMR (DMSO, 75 MHz) δ (ppm): 39.56 (CH₃), 99.7, 101.41, 104.33, 109.12, 112.33, 118.5, 121.48, 127.3, 129.43, 129.91, 137.66, 138.7, 139.2, 146.45, 152.49, 157.26, 161.7 (SP² carbon atoms); Anal. Calcd for C₂₀H₁₄ClN₅ (359.09): C, 66.85; H, 3.90; N, 19.50%. Found: C, 66.65; H, 3.74; N, 19.88%.

7-(4-Chlorophenyl)-3-methyl-9-phenyl-7H-pyrrolo[3,2-e][1,2,4]triazolo[4,3-c]pyrimidine (5b)

Yield: 63%; m.p.: 201–203 °C; IR (KBr) ν (cm⁻¹): 1572 (C=N); MS (EI) m/z : 361 (M + 2, 10.7%), 359 (M⁺, 30.33%), ¹H NMR (DMSO-d₆, 300 MHz) δ (ppm): 2.50 (s, 3H, C3-CH₃), 6.51–7.56 (m, 10H, Ar-H), 8.61 (s, 1H, C5-H); Anal. Calcd for C₂₀H₁₄ClN₅ (359.09): C, 66.85; H, 3.90; N, 19.50%. Found: C, 66.88; H, 4.05; N, 19.64%.

General procedure for the synthesis of compounds 6(a–b)

A solution of the appropriate hydrazine **2(a–b)** (0.01 mol) in pyridine (10 mL) was cooled in an ice bath, and an equimolar amount (0.01 mol) of ethyl chloroformate was added portion wise. Then the mixture was heated under reflux for 3 h, cooled, poured onto ice water and neutralised with HCl to give a precipitate which was filtered off, dried and recrystallized from ethanol to yield compounds **6(a–b)**.

7-(3-Chlorophenyl)-9-phenyl-7H-pyrrolo[3,2-e][1,2,4]triazolo[4,3-c]pyrimidin-3-one (6a)

Yield: 59%; m.p.: 226–228 °C; IR (KBr) ν (cm⁻¹): 3402 (N–H), 1673 (C=O), 1512 (C=N); MS (EI) m/z : 361 (M + 2, 10.84%), 359 (M⁺, 29%), ¹H NMR (DMSO-d₆, 300 MHz) δ (ppm): 6.26–7.84 (m, 11H, Ar-H), 7.87 (s, 1H, NH, D₂O exchangeable); Anal. Calcd for C₁₉H₁₂ClN₅O (359.07): C, 63.16; H, 3.32; N, 19.39%. Found: C, 63.31; H, 3.35; N, 19.35%.

7-(4-Chlorophenyl)-9-phenyl-7H-pyrrolo[3,2-e][1,2,4]triazolo[4,3-c]pyrimidin-3-one (6b)

Yield: 63%; m.p.: 233–235 °C; IR (KBr) ν (cm⁻¹): 3390 (N–H), 1681 (C=O), 1520 (C=N); MS (EI) m/z : 363 (M + 2, 8.87%), 361 (M⁺,

26.78%), ¹H NMR (DMSO-d₆, 300 MHz) δ (ppm): 6.90–7.87 (m, 11H, Ar-H), 8.31 (s, 1H, NH, D₂O exchangeable); ¹³C-NMR (DMSO, 75 MHz) δ (ppm): 98.04, 102.43, 109.14, 115.6, 116.49, 127.5, 129.20, 129.55, 130.48, 131.60, 133.42, 138.3, 157.41, 162.0 (SP² carbon atoms), 166.91 (C=O), Anal. Calcd for C₁₉H₁₂ClN₅O (361.07): C, 63.16; H, 3.32; N, 19.39%. Found: C, 63.15; H, 3.66; N, 19.02%.

General procedure for the synthesis of compounds 7(a–b)

A mixture of the appropriate hydrazine **2(a–b)** (0.01 mol) and acetyl acetone (0.01 mol) in absolute ethanol was heated under reflux for 3 h, cooled, poured onto ice water to give a precipitate which was filtered off, dried, and recrystallized from ethanol to yield compounds **7(a–b)**.

7-(3-Chlorophenyl)-4-(3,5-dimethyl-pyrazol-1-yl)-5-phenyl-pyrrolo[2,3-d]pyrimidine (7a)

Yield: 45%; m.p.: 180–182 °C; IR (KBr) ν (cm⁻¹): 1608 (C=N); MS (EI) m/z : 401 (M + 2, 7.01%), 399 (M⁺, 20.68%), ¹H NMR (DMSO-d₆, 300 MHz) δ (ppm): 2.05 (s, 3H, CH₃), 2.39 (s, 3H, CH₃), 6.92–7.89 (m, 11H, Ar-H), 8.32 (s, 1H, C-2 H); Anal. Calcd for C₂₃H₁₈ClN₅ (399.12): C, 69.17; H, 4.51; N, 17.54%. Found: C, 69.20; H, 4.79; N, 17.35%.

7-(4-Chlorophenyl)-4-(3,5-dimethyl-pyrazol-1-yl)-5-phenyl-pyrrolo[2,3-d]pyrimidine (7b)

Yield: 53%; m.p.: 199–201 °C; IR (KBr) ν (cm⁻¹): 1617 (C=N); MS (EI) m/z : 401 (M + 2, 6.73%), 399 (M⁺, 19.3%), ¹H NMR (DMSO-d₆, 300 MHz) δ (ppm): 2.03 (s, 3H, CH₃), 2.36 (s, 3H, CH₃), 6.88–7.84 (m, 11H, Ar-H), 8.31 (s, 1H, C-2 H); Anal. Calcd for C₂₃H₁₈ClN₅ (399.12): C, 69.17; H, 4.51; N, 17.54%. Found: C, 69.36; H, 4.32; N, 17.66%.

General procedure for the synthesis of compounds 8(a–f)

A mixture of the appropriate hydrazine **2(a–b)** (0.01 mol) and aromatic aldehyde (0.01 mol) was heated under reflux in absolute ethanol for 8 h, cooled, poured onto ice water to give precipitates which were filtered off, dried and recrystallized from ethanol to give compounds **8(a–f)**.

N-[(E)-benzylideneamino]-7-(3-chlorophenyl)-5-phenyl-pyrrolo[2,3-d]pyrimidin-4-amine (8a)

Yield: 46%; m.p.: 187–189 °C; IR (KBr) ν (cm⁻¹): 3323 (N–H), 1608 (C=N); MS (EI) m/z : 423 (M + 2, 20.45%), 421 (M⁺, 63.43%), ¹H NMR (DMSO-d₆, 300 MHz) δ (ppm): 5.43 (s, 1H, NH, D₂O exchangeable), 6.43–7.94 (m, 15H, Ar-H), 8.26 (s, 1H, C-2 H), 8.51 (s, 1H, CH); Anal. Calcd for C₂₅H₁₈ClN₅ (421.12): C, 70.92; H, 4.26; N, 16.55%. Found: C, 70.82; H, 4.51; N, 16.36%.

N-[(E)-benzylideneamino]-7-(4-chlorophenyl)-5-phenyl-pyrrolo[2,3-d]pyrimidin-4-amine (8b)

Yield: 60%; m.p.: 172–174 °C; IR (KBr) ν (cm⁻¹): 3345 (N–H), 1598 (C=N); MS (EI) m/z : 425 (M + 2, 7.01%), 423 (M⁺, 21.61%), ¹H NMR (DMSO-d₆, 300 MHz) δ (ppm): 5.21 (s, 1H, NH, D₂O exchangeable), 6.79–7.53 (m, 16H, Ar-H), 7.95 (s, 1H, CH); Anal. Calcd for C₂₅H₁₈ClN₅ (423.12): C, 70.92; H, 4.26; N, 16.55%. Found: C, 70.69; H, 4.20; N, 16.35%.

7-(3-Chlorophenyl)-N-[(E)-(4-chlorophenyl)methyleneamino]-5-phenyl-pyrrolo[2,3-d]pyrimidin-4-amine (8c)

Yield: 65%; m.p.: 247–249 °C; IR (KBr) ν (cm⁻¹): 3331 (N–H), 1618 (C=N); MS (EI) m/z : 459 (M + 4, 3.3%), 457 (M + 2, 31.51%), 455 (M⁺, 47.38%), ¹H NMR (DMSO-d₆, 300 MHz) δ (ppm): 5.99 (s, 1H, NH, D₂O exchangeable), 6.62–7.91 (m, 15H, Ar-H), 8.63 (s, 1H, CH); Anal. Calcd for C₂₅H₁₇Cl₂N₅ (455.08): C, 65.65; H, 3.72; N, 15.32%. Found: C, 65.80; H, 4.08; N, 15.37%.

7-(4-Chlorophenyl)-N-[(E)-(4-chlorophenyl)methyleneamino]-5-phenyl-pyrrolo[2,3-d]pyrimidin-4-amine (8d)

Yield: 68%; m.p.: 187–189 °C; IR (KBr) ν (cm⁻¹): 3338 (N–H), 1602 (C=N); MS (EI) m/z : 461 (M + 4, 2.61%), 459 (M + 2, 17.21%), 457 (M⁺, 25.61%), ¹H NMR (DMSO-d₆, 300 MHz) δ (ppm): 4.48 (s, 1H, NH, D₂O exchangeable), 6.71–7.90 (m, 15H, Ar-H), 8.35 (s, 1H, CH); Anal. Calcd for C₂₅H₁₇Cl₂N₅ (457.08): C, 65.65; H, 3.72; N, 15.32%. Found: C, 65.55; H, 3.70; N, 15.36%.

7-(3-Chlorophenyl)-N-[(E)-(4-methoxyphenyl)methyleneamino]-5-phenyl-pyrrolo[2,3-d]pyrimidin-4-amine (8e)

Yield: 72%; m.p.: 167–169 °C; IR (KBr) ν (cm⁻¹): 3418 (N–H), 1604 (C=N); MS (EI) m/z : 455 (M + 2, 23%), 453 (M⁺, 67.39%), ¹H NMR (DMSO-d₆, 300 MHz) δ (ppm): 3.42 (s, 1H, OCH₃), 5.26 (s, 1H, NH, D₂O exchangeable), 6.71–7.66 (m, 15H, Ar-H), 7.88 (s, 1H, CH); Anal. Calcd for C₂₆H₂₀ClN₅O (453.13): C, 68.87; H, 4.42; N, 15.45%. Found: C, 68.87; H, 4.61; N, 15.44%.

7-(4-Chlorophenyl)-N-[(E)-(4-methoxyphenyl)methyleneamino]-5-phenyl-pyrrolo[2,3-d]pyrimidin-4-amine (8f)

Yield: 80%; m.p.: 194–196 °C; IR (KBr) ν (cm⁻¹): 3407 (N–H), 1605 (C=N); MS (EI) m/z : 455 (M + 2, 8.91%), 453 (M⁺, 25.35%), ¹H NMR (DMSO-d₆, 300 MHz) δ (ppm): 4.12 (s, 1H, OCH₃), 4.50 (s, 1H, NH, D₂O exchangeable), 6.89–8.18 (m, 15H, Ar-H), 8.28 (s, 1H, CH); Anal. Calcd for C₂₆H₂₀ClN₅O (453.13): C, 68.87; H, 4.42; N, 15.45%. Found: C, 68.77; H, 4.34; N, 15.17%.

Molecular docking

All compounds were constructed using MOE 2014.09 and filed in a molecular database file³⁹. The crystal structure of COX-2 TLR-2 and TLR-4 were downloaded from the protein data bank (PDBID: **4COX**, **2Z80** and **2Z63**; respectively)^{40–42}. Protein was energy diminished and 3D protonated *via* the structure preparation module of MOE. The co-crystallized bound compound and water molecules were removed from the crystal structure. The site of docking was recognised and the database containing all the tested compounds has been established using rigid receptor as a docking protocol and triangle matcher as a placement method. Two rescoring functions were selected, London dG and GBVI/WSA dG. The force field was used as a refinement. Free binding energy (kcal/mol) was calculated, and only the best-scored pose was selected for each compound.

Molecular dynamic simulation

Four molecular dynamic simulations (MDS) were conducted for 100 ns using GROMACS 2.1.1 software⁴³. The retrieved docking coordinates of COX-2 and TLR-4 bound to **4b** and **8e** were used as input structures for the molecular dynamics. The receptor and ligand topologies were generated by PDB2gmX (embedded in GROMACS) and GlycoBioChem PRODRG2 Server respectively, both under GROMOS96 force field⁴⁴. After rejoining ligands and receptor topologies to generate the four systems, the typical molecular

dynamics scheme of GROMACS was applied for all the systems. This includes solvation, neutralisation, energy minimisation under GROMOS96 43a1 force field and two stages of equilibration (NVT and NPT)⁴⁵. Finally, unrestricted production stage of 100 ns was applied for the four systems with particle mesh ewald (PME) method implemented to compute the long-range electrostatic values using 12 Å cut-off and 12 Å Fourier spacing. The stability of the complexes was judged using RMSD and RMSF values calculated from the MDS trajectories from the production step.

MM-PBSA calculation and per residue contribution

The MM-PBSA package of Kumari et al.⁴⁶ was contrived to calculate the binding free energy between the ligands and the two receptors using the following equation. All four complexes were subjected to such calculations.

$$\Delta G_{(\text{Binding})} = G_{(\text{Complex})} - G_{(\text{Receptor})} - G_{(\text{Ligand})}$$

Biology

Antioxidant activity of tested compounds using 2,2-Diphenyl-1-picrylhydrazyl (DPPH) radical scavenging protocol

DPPH scavenging potential of samples was determined with a slightly modified method^{47,48}. Each sample was prepared at 500 ppm. Serial concentrations of samples were prepared (200 μ L, 400 μ L and 800 μ L). Methanol was added to complete the total volume to 1 mL and all the samples were vortexed well. 1 mL of 0.1 mM DPPH methanolic solution was added to each diluted sample. All the samples were vortexed again, then left to stand for 30 min in the dark at environment temperature. The absorption of the developed colour appeared against the blank reagent was measured at 517 nm using a spectrophotometer. BHT was used as a standard antioxidant. The capability to scavenge DPPH radical was estimated using the following equation:

$$\text{DPPH scavenging ability (\% inhibition)} = [(A_0 - A^*)/A_0] \times 100$$

A₀ is Control absorption and A* is sample absorption.

Anti-inflammatory activity

Cell culture (seeding and treatment)

The macrophage cell line, RAW 264.7 was obtained from the ATCC (American type culture collection). The cells were cultured in RPMI 1640 medium (Roswell Park Memorial Institute) and supplemented with 1% pen/strep and 10% heat-inactivated foetal bovine serum. The cells were incubated, in a humidified incubator, in an atmosphere of 5% CO₂ at 37 °C and were subculture twice before the experiment⁴⁹.

RAW 264.7 cells were suspended in a RPMI medium. After 24 h of seeding 1 × 10⁵ cells per well (in 96 well plates) and incubated for 24 h for the experiments. The cells were then treated with the samples at concentrations of 100, 50, 25 and 12.5 μ g/mL and incubated for 1 h. They were then stimulated with 10 μ g/mL of LPS for another 24 h. The supernatant was gently transferred to new 96-well plates and used for NO determination, while the cells that remained in the old plate were used for the MTT assay of cell viability. Samples (stock) were dissolved in DMSO, and the working samples were prepared in the media. Cell viability was assessed by the mitochondrial dependent reduction of yellow MTT (3-(4,5-dimethylthiazol-2-yl)-2,5-diphenyltetrazolium bromide) to purple formazan⁴⁹.

The percentage of change in viability was calculated according to the formula:

$$\left[\left(\frac{\text{Reading of extract}}{\text{Reading of negative control}} \right) - 1 \right] \times 100.$$

Nitric oxide assay

Nitric oxide production was assayed by measuring nitrite in the supernatants of cultured LPS-RAW 264.7 cells. The assay was carried out as described previously with slight modification^{48,50}. After pre-incubation of RAW 264.7 cells (1×10^5 cells/mL) with LPS (10 $\mu\text{g/mL}$) for 24 h, the amount of nitrite, a stable metabolite of NO used as an indicator of NO production in the culture medium was measured using the Griess reagent (1% sulphanilamide and 0.1% naphthyl ethylenediamine dihydrochloride in 2.5% phosphoric acid). A volume of 50 μL of the cell culture medium was mixed with 50 μL of the Griess reagent. Subsequently, the mixture was incubated at room temperature for 15 min and the absorbance was measured at 540 nm by a microplate reader. Fresh culture medium was used as a blank in every experiment. The quantity of nitrite was determined from a sodium nitrite standard curve as expressed in the equation.

$$\text{Nitric oxide inhibition (\%)} = \left(\frac{\text{optical density of control} - \text{optical density of test}}{\text{optical density of control}} \right) \times 100.$$

Results

Chemical results

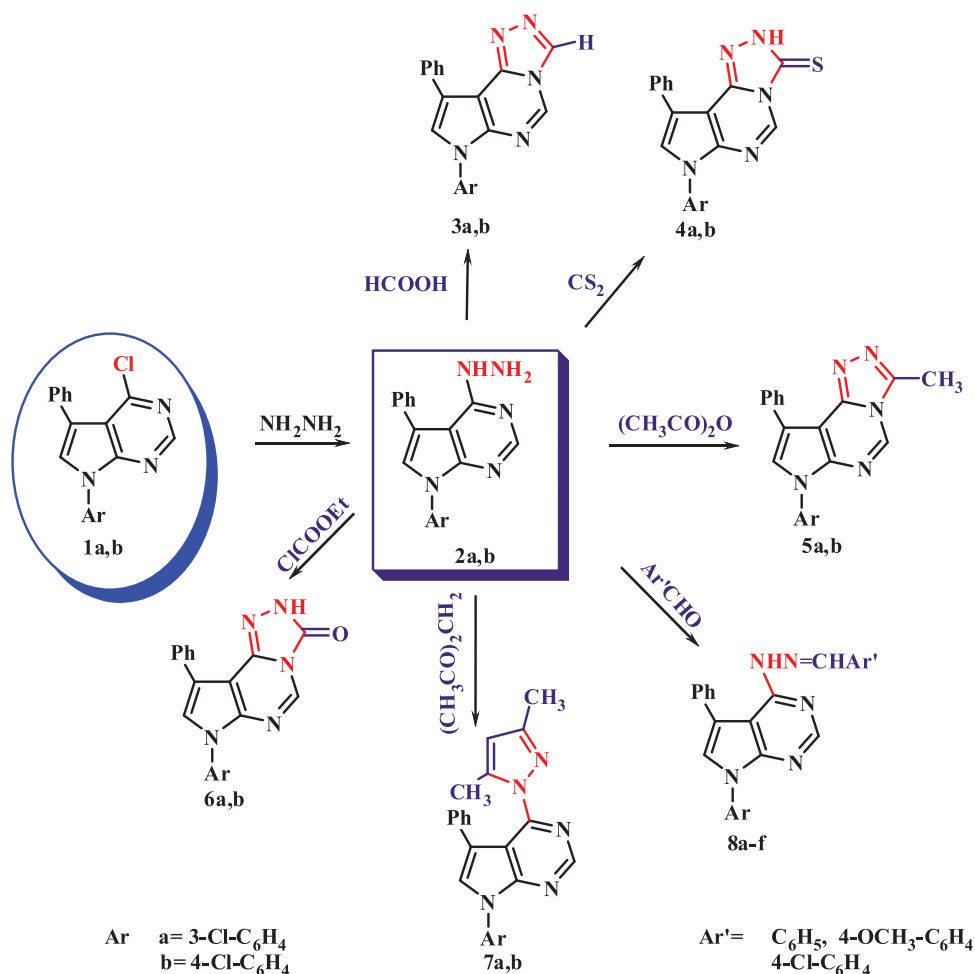
The remarkable biological activity of pyrrolopyrimidines and fused pyrrolopyrimidine derivatives^{51–54} has inspired us to synthesise

new derivatives and test their anti-inflammatory activity^{55,56}. The synthetic strategies for our target compounds are presented in Scheme 1.

The previously reported 4-chloropyrrolopyrimidine derivatives **1(a–b)** were heated under reflux, independently, with hydrazine hydrate in absolute ethanol to afford 4-hydrazino-pyrrolopyrimidines **2(a–b)**, which were subsequently used as starting materials for the other novel derivatives^{38,57}. In brief, pyrrolo[3,2-*e*][1,2,4]triazolo[4,3-*c*]pyrimidine derivatives **3(a–b)** and **6(a–b)** were obtained via reaction of hydrazino derivatives **2(a–b)** with formic acid, CS_2 , acetic anhydride and ethyl chloroformate, respectively^{52,58}. Analysis of the spectral data of the new compounds confirm their structure in many features; as the disappearance of NH_2 group absorption bands in IR spectra as well as its signal in $^1\text{H-NMR}$ spectra, also that of NH group in some of these compounds, increasing number of aromatic protons, the appearance of amide or thioamide distinctive peaks. Additionally, 4-Hydrazino derivatives **2(a–b)** were also reacted with acetylacetone to produce 4-pyrazolyl-pyrrolopyrimidines **7(a–b)**. Finally, *N*-(arylidineamino)-pyrrolopyrimidine-4-amines **8(a–f)** were obtained from the condensation reaction of **2(a–b)** with different aromatic aldehydes. The structures of all the produced compounds were supported with elemental analysis and spectral data^{51,53}.

Biological evaluation

In this study, we examined the effect of 18 newly synthesised compounds against reactive oxygen species (ROS), using 1,1-diphenyl-2-picrylhydrazyl (DPPH) radical scavenging assay using a well-known antioxidant control drug butylated hydroxytoluene (BHT). BHT is a lipophilic organic compound frequently used



Scheme 1. Synthesis of Pyrrolopyrimidines and Pyrrolotriazopyrimidines (2–8).

antioxidant recognised as safe for use in foods, pharmaceuticals and different industries^{49,59}. Three compounds (namely **triazolo-pyrrolopyrimidines 3a, 4b**, and **arylidineaminopyrrolopyrimidine 8e**) showed significant activity against the standard reference (BHT).

The DPPH assay is the commonly used assay to define the promising antioxidant compounds, which act as free radical scavengers *in vitro*⁶⁰. All the tested compounds exhibited poor or no scavenging properties against the DPPH radical, except for three compounds (**3a, 4b**, and **8e**) and the %inhibition was proportional to the concentration of each compound. Compounds **3a, 4b**, and **8e** showed promising anti-oxidative activities compared to the reference, BHT. Compound **8e** revealed the premier DPPH-scavenging activity, followed by compounds **4b** and **3a** as shown in Table 1.

According to the data in Table 1, the ideal radical-scavenging activity of our samples was demonstrated by compound **8e** at concentration 200 µg/mL which provides the highest antioxidant activity when compared to the same concentration of BHT. Compound **4b** also exhibited significant activity (with IC₅₀ ≈ 129 µg/mL), which is similar to that of BHT followed by compound **3a** (IC₅₀ ≈ 160 µg/mL).

The determination of the cytotoxic effect of our active antioxidant compounds on normal macrophages was critical, as shown in previous studies, many bioactive compounds were reported as toxic agents to normal cells and could be responsible for cells death by disrupting protein synthesis^{48–50,61}. Table 2 shows the possible cytotoxic activity of our active compounds against macrophage cell line RAW 264.7.

As shown in Table 2, the highest cytotoxic activity was observed by compound **3a** at a concentration of 100 µg/mL and the lowest cytotoxic activity was observed by compound **8e** at a concentration of 25 µg/mL. The cytotoxic activity of our compounds could be attributed to a variety of factors, including the induction of cell damage, the initiation of various immune system reactions, and the electrostatic attraction of sample, and treated cells. These findings suggest that their cytotoxicity was most likely caused by low glutathione levels, high lipid peroxidation, and reactive oxygen species in responsive genes, which caused DNA damage and necrosis, followed by the evaluation of nitric oxide (NO) production and LPS-induced cytotoxicity and inflammatory response in RAW 264.7.

The effect of different concentrations of our tested compounds on nitric oxide (NO) was investigated using the Griess assay to estimate nitrite accumulation in the cultivating medium^{48,62–66}.

The data presented in Table 3 demonstrated that our compounds significantly inhibited LPS- stimulated NO production by LPS- induced RAW 264.7 macrophages. The highest inhibition activity was observed by compound **8e** at IC₅₀ ≈ 53 µg/mL

Discussion

Inflammation and oxidative stress are considered exceptionally related events; both are considered the main factor in many chronic diseases as lung injury and COVID-19. Moreover, increasing evidence shows that oxidative stress is recognised as the key path-way affecting the severity of lung injury^{13,67–69}. Macrophages play critical roles in the initiation of inflammatory responses through secretion of a great number of pro-inflammatory mediators and cytokines, including tumour necrosis factor-α (TNF-α), interleukin-1β (IL-1β), IL-6, inducible nitric oxide synthase (iNOS) and cyclooxygenase-2 (COX-2)^{14,70–72}. In early responses to inflammation, specific damage-associated molecular patterns are

Table 1. DPPH radical-scavenging activity of active compounds^a against reference anti-oxidant BHT.

Conc.	Active comp.			
	% Inhibition (mean ± SEM)			
	100	200	400	IC ₅₀ µg/mL
3a	39.56 ± 0.88	58.09 ± 1.50	62.51 ± 0.32	160.05
4b	37.97 ± 0.71	77.76 ± 1.60	79.55 ± 1.06	129.38
8e	40.63 ± 2.13	82.15 ± 0.14	85.22 ± 0.17	122.07
BHT	40.03 ± 0.39	76.81 ± 0.21	90.07 ± 0.26	128.77

^aAll compounds (3–8) were tested against DPPH; result represent the most active compounds.

Table 2. Cytotoxicity of compounds **3a, 4b** and **8e** against RAW macrophage cells.

Active comp.	Cytotoxicity of raw cells% (mean ± SEM)			
	100 µg/mL	50 µg/mL	25 µg/mL	12.5 µg/mL
3a	92.0 ± 1.6	78.7 ± 2.2	76.5 ± 1.9	0
4b	85.4 ± 0.6	75.2 ± 2.5	69.6 ± 1.3	0
8e	77.7 ± 1.5	73.1 ± 1.3	65 ± 3.1	0
LPS (–ve control)	–	–	–	–

Table 3. Anti-inflammatory activity of compounds **3a, 4b** and **8e** against nitric oxide.

Conc.	Comp.				
	NO % inhibition (mean ± SEM)				
	100 µg/mL	50 µg/mL	25 µg/mL	12.5 µg/mL	IC ₅₀ µg/mL
3a	65.6 ± 1.2	62.5 ± 1.2	53.1 ± 1.3	40.6 ± 2.6	57.3
4b	58.1 ± 3.5	54.3 ± 1.6	52.8 ± 1.1	39.8 ± 1.9	64.8
8e	71.8 ± 1.0	67.5 ± 1.8	66.5 ± 3.7	38.7 ± 1.7	52.5

recognised by immune cell pattern recognition receptors (PRRs), including toll-like receptors (TLRs), pattern recognition receptors (PRR) recognise pathogen-associated molecular patterns (PAMPs)^{73–75}. TLR-4 can be also activated by damage-associated molecular patterns (DAMPs) and endogenous agonists released by injured tissues and necrotic cells^{76–82}. TLR4-mediated inflammation, triggered by DAMPs, is involved in several diseases such as sepsis. Sepsis is one of the potential medical complications in severe influenza and recently in SAR-CoV-2 infection; leading to life-threatening organ dysfunction⁷.

Septic shock with overexpression of pro-inflammatory cytokines could be competently blocked by using TLR4 antagonists. Selective TLR4 antagonists as Eritoran (E5564) and TAK-242 were first progressed to clinical trials for the treatment of sepsis and have been discontinued in different phases. Yet, due to COVID–19 pandemic crisis, Eisai Co., Ltd. is participating in the global network REMAP-CAP-COVID (Randomized, Embedded, Multi-factorial, Adaptive Platform-Community Acquired Pneumonia COVID), which aims at developing therapeutics drugs for the novel coronavirus through drug repurposing, hoping to control the cytokine storm and prevent pneumonia complications through inhibiting the activation of TLR4 located at the uppermost stream of various cytokine production signals that cause cytokine storms, involved in the aggravation of pneumonia caused by coronavirus⁶⁷.

Based on the nature of LPS, a hydrophobic lipid A domain, as TLRs agonist; several synthetic compounds have been developed as adjuvants for clinical use (namely; small-molecule inhibitors, peptides, microRNAs, nanoparticles, lipid A analogs, and derivatives of natural products)^{79,80,83–86}. Recently, a bivalent ligands containing pharmacophores derived from naltrexone has reported showing a high selectivity. The MD-2 binding pocket is much

larger than the size of (+)-naltrexone, which allows the discovery of ligand dimerisation of two bivalent ligands by connecting two naltrexone units through a rigid pyrrole spacer. Screening of clinically approved drugs with high blood – brain barrier permeability was also considered due to the high failure rate of new TLR-4 antagonist. Lovastatin, a well-known anti-hyperlipidemic drug, was recognised as a specific TLR4 antagonist, small-molecule acting as TLR-4 antagonist, can either block ligand-receptor interaction or cause dimerisation of the TLR4-MD2 complex. As an example; TAK-242 (resatorvid), a cyclohexane derivative that binds to the SH₂ group of cysteine of the TIR domain. A previously reported compound T5342126 (Figure 2), as a selective TLR4 inhibitor was found to be an inhibitor of the interaction interface of TLR4-MD2^{61,87–91}. Molecular docking was performed and revealed that the benzyl group of this compound binds with the hydrophobic pocket of TLR4, and the carbazole group occupies the MD2 pocket.

New approaches to the relation between TLRs and COX-2 also investigated several inflammatory pathways including inflammatory arthritis, cancer and diabetic nephropathy^{92–96}. Experiments using TLR2 deficient, TLR4-deficient, and NLRP3-deficient mice indicated that these three proteins are involved in macrophage prostaglandin E2 (PGE2) secretion. Also, it has been reported that the immune responses to induced brain abscesses did not only depend on TLR2 but also TLR4 was required, suggesting that they play key roles in immune response modulation, inflammation, and induced PGE2; an endogenous lipid mediator that is essential for pathological conditions, immune cell secretion of different organs and also act as an inflammatory mediator. Sign for response to the acute inflammatory stimulation, are the release of prostaglandins (PG), and leukotrienes. In which the inhibition of PGE synthesis is considered an important anti-inflammatory strategy^{93,97,98}. PGE2 is generated by the conversion of arachidonic acid (AA), which is released and used by 2 different cyclooxygenases (COXs),

COX-1 (constitutive) and COX-2 (inducible)^{53,74,88,89,91,99–104}. COX-2 is responsible for prostaglandin production during different pathological processes involving inflammation^{97,98,105}. Recently, it is assumed that inflammation can lead to carcinogenesis by generation of ROS that can damage DNA, and excessive production of cytokines, which will regulate the COX-2/PGE2 (prostaglandin E2) signal pathway in inflammation and cancer cells^{93,97,98,106}. Providing new evidence through the inhibition of inflammatory cytokine expression, which can aid in diminish tumour development and progression. NSAIDs are investigated for the prevention of cancer progression and metastasis, particularly in the case of colon cancer^{97,98}.

Many pathways have been reported for the LPS-macrophages activated by the TLR4 agonist and/or induced by TLR2/MyD88 activation, which is important for inflammatory processes are characterised by increased COX-2 accounting for the bulk of PGE biosynthesis^{93,107}. NSAIDs inhibit both COXs enzymes and decrease production of PGE2 among these pyrrole containing compounds^{108–110}. These compounds block PGE synthesis by non selective inhibition (indomethacin, acemetacin, tolmetin and ketorolac) or by selective-inhibition of COX-2 (etodolac). Although the overmentioned importance, lately the concern about drug interactions between widespread NSAIDs and cardiovascular treatments has been provided in several clinical settings^{111,112}. The cardiovascular safety of NSAIDs have arisen initially because of reported associations between rofecoxib (COX-2 selective inhibitor) and myocardial infarction, causing rofecoxib to withdrawn from market in 2004¹¹³. Others COX-2-selective inhibitors, namely; celecoxib, valdecoxib, parecoxib, etoricoxib and lumiracoxib. All have shown a reduced risk of inducing gastroduodenal injury. Cardiovascular risk was also reported in for celecoxib, yet the evidence showed that the cardiovascular risks of celecoxib is less than that with rofecoxib, appeared to be dependent on the individual drugs. New compounds have been added to NSAIDs a day on to

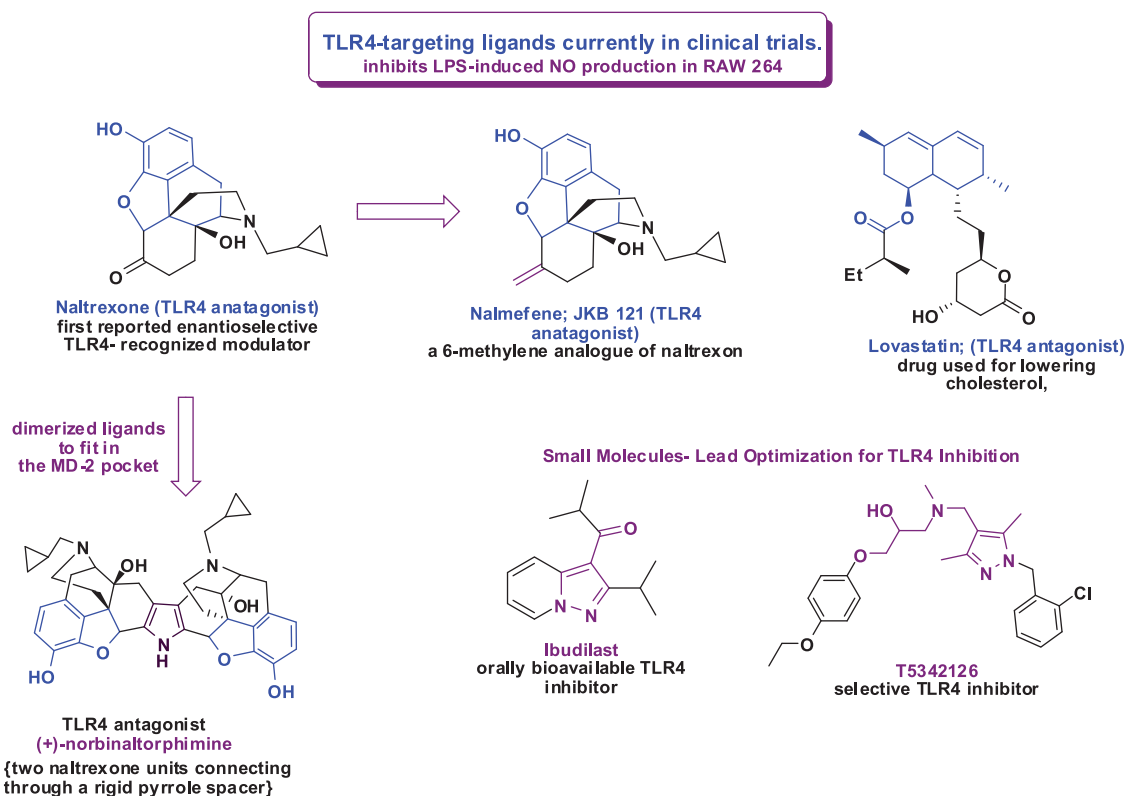


Figure 2. TLR4-targeting ligands currently in clinical trials.

overcome the mention side effects among theses and in order drug discovery of new anti-inflammatory drugs with high safety targeting the TLRs as new potent anti-inflammatory novel compounds.; among these a series of *N*-pyrrolylcarboxylic acids have been reported as potent COX-2 inhibitors^{114,115}, as revealed in (Figure 3).

To understand the biological results presented herein of our active compounds, a molecular docking study was performed using the MOE 2014.09 software. Molecular docking screenings were performed after achieving synthesis and characterisation of the all-new compounds. The potential binding modes for the most active compounds (**3a**, **4b**, and **8e**) was explored within the active site of the COX-2; both TLR-2 and TLR-4 were used. The

binding affinity of the highly active compounds was calculated inside all the three enzymes' binding sites^{73,83,89} as shown in Figures 4–6.

The binding modes of the active compounds inside the active site of COX-2 were evaluated using the protein coordinates (PDB 4COX) of COX-2 in bound with its ligand (Indomethacin). All the newly synthesised compounds were docked into the active site of COX-2. The results confirmed that the three compounds: triazolo-pyrrolopyrimidines **3a**, **4b**, and arylideneaminopyrrolo-pyrimidine **8e** had the lowest clash score, which confirm their well-fitting in the binding site and resulted in the highest affinity values within MOE 2014.09 docking results as revealed in Figure 4.

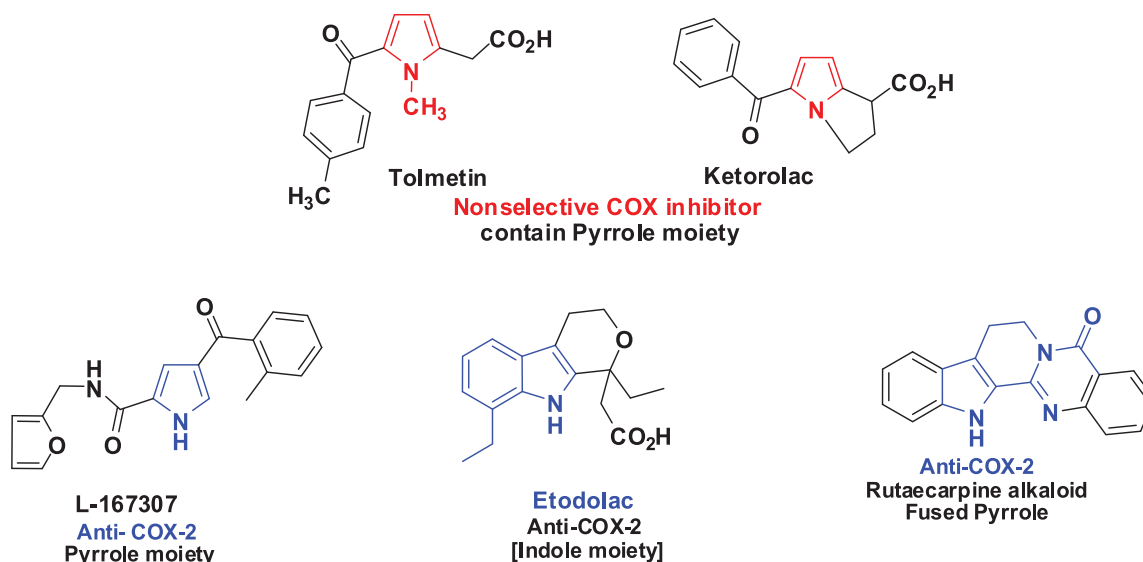


Figure 3. Pyrrole and fused pyrrole as selective COX-2 inhibitor³¹.

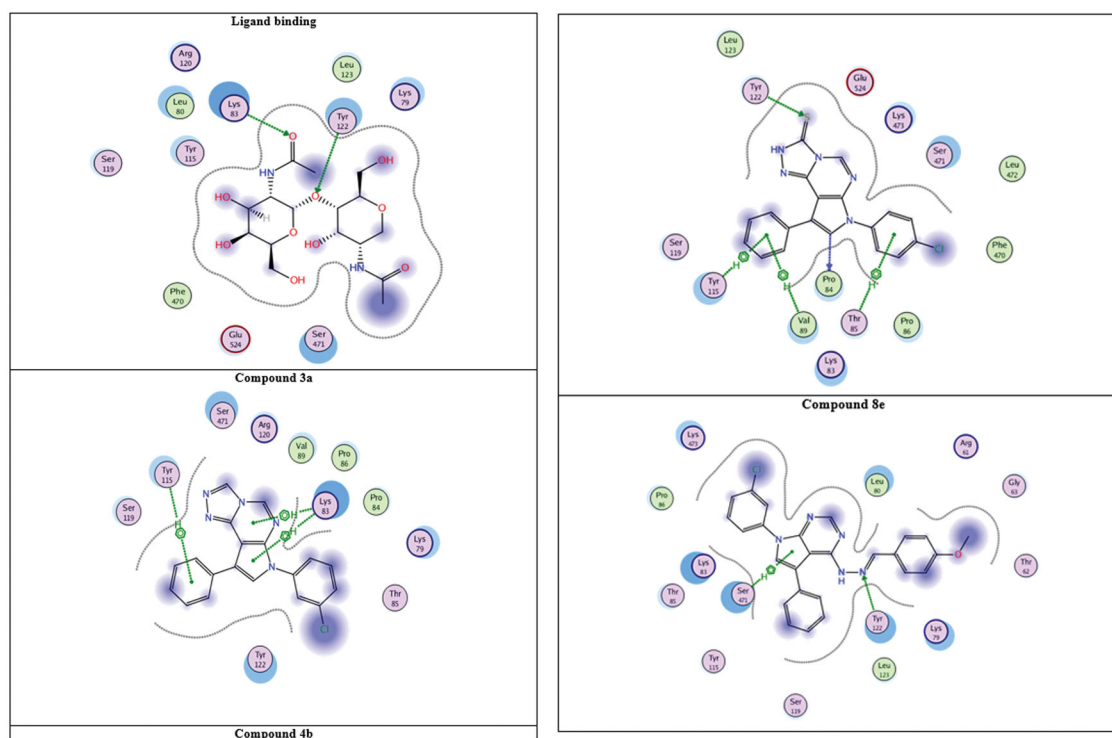


Figure 4. The binding modes of the active compounds with COX-2 active site.

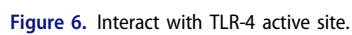
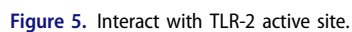


Table 4. Results for molecular docking studies of compounds **3a**, **4b** and **8e** versus reference in COX-2 active site (PDB: 4COX).

Compound	Docking score (s) Kcal/mol	RMSD	E score 1 (London dG) Kcal/mol	E score 2 (London dG) Kcal/mol	Binding interaction (ligand-receptor)
3a	−4.8144	1.9552	−8.0943	−4.8144	(Pyrimidine-LYS83) (pi-H, 3.54 Å) (Pyrrole-LYS83) (pi-H, 3.87 Å) (Benzene-TYR115) (pi-H, 3.70 Å)
4b	−5.2967	1.3831	−8.4435	−5.681	(Pyrrole C-PRO84) (H-b, 2.82 Å) (S-TYR122) (H-b, 3.09 Å) (7-Benzene-THR85) (pi-H, 3.91 Å) (9-Benzene-VAL89) (pi-H, 3.95 Å) (9-Benzene-TYR115) (pi-H, 3.50 Å)
8e	−5.4527	1.5696	−8.6607	−5.4527	(N arylidine-TYR122) (H-b, 3.00 Å) (Pyrrole-SER471) (pi-H, 3.66 Å)
Ligand (indomethacin)	−4.3598	2.4889	−9.9341	−4.3598	(O-TYR122) (H-b, 2.88 Å) (O-LYS83) (H-b, 2.83 Å)

Table 5. Results for molecular docking studies of compounds **3a**, **4b** and **8e** versus reference in TLR-2 active site (PDB: 2Z80).

Compound	Docking score (s) Kcal/mol	RMSD	E score 1 (London dG) Kcal/mol	E score 2 (London dG) Kcal/mol	Binding interaction (ligand-receptor)
3a	−5.1732	1.2973	−7.7491	−4.5062	(Cl-ASPB106) (H-b, 3.14 Å) (Triazole -THRA262) (pi-H, 3.82 Å)
4b	−4.1056	0.9909	−7.353	−4.1056	(N-ASPA235) (H-b, 3.18 Å) (Pyrimidine-ASPB31) (pi-H, 3.68 Å) (Triazole-ASPB31) (pi-H, 3.93 Å)
8e	−5.6498	1.7683	−8.3973	−5.7715	(Benzene-ASPB31) (pi-H, 3.94 Å) (Benzene-LYSB37) (pi-H, 3.55 Å)
Ligand	−3.6659	2.6939	−8.0864	−3.667	(O-GLNA209) (H-b, 3.11 Å) (O-LYSB37) (H-b, 3.20 Å) (O-GLYB41) (H-b, 3.16 Å)

Table 6. Results for molecular docking studies of compounds **3a**, **4b** and **8e** versus reference in TLR-4 active site (PDB: 2Z63).

Compound	Docking score (s) Kcal/mol	RMSD	E score 1 (London dG) Kcal/mol	E score 2 (London dG) Kcal/mol	Binding interaction (ligand-receptor)
3a	−4.2663	1.5633	−8.003	−4.2663	(Benzene-GLU89) (pi-H, 3.75 Å) (Pyrimidine-PRO113) (pi-H, 3.82 Å) (Triazole-PRO113) (pi-H, 3.50 Å)
4b	−5.5773	1.4679	−8.1094	−4.575	(Triazole-GLU89) (pi-H, 3.98 Å) (Pyrrole-PRO113) (pi-H, 3.77 Å) (Benzene-PRO113) (pi-H, 3.83 Å) (Benzene-ASN137) (pi-H, 3.54 Å)
8e	−4.2089	1.5556	−7.8398	−4.2089	(Cl-GLU42) (H-b, 3.87 Å) (N Pyrimidine-GLU89) (H-b, 3.55 Å)
Ligand	−4.0874	1.9803	−8.1268	−3.7956	(O-ASN137) (H-b, 3.20 Å) (O-GLU89) (H-b, 3.07 Å)

As shown in Figure 4 and Table 4, the reference ligand forms hydrogen bonding with both Tyr 122 and Lys 83 amino acid residues as the main non-covalent interactions with the protein. Compound **4b** showed the highest binding affinity, forming an H-bond with both of the Tyr 122 and Pro 84 amino acid residues. Furthermore, three more hydrophobic interactions were recognised with Tyr 115, Val 89 and Thr 85 amino acid residues. Compound **8e** shows good binding affinity resulting from both hydrophobic interaction with Ser 471 and hydrophilic hydrogen bonding (using hydrazine N) with Tyr 122 amino acid residue. For compound **3a**, two hydrophobic interactions were observed with Lys 83 and Tyr 115 amino acid residues. The *in silico* results of compounds **3a**, **4b** and **8a** were promising and a further investigation of three compounds using DPHH and NO assay was performed as previously mentioned. The three compounds showed promising *in-vitro* activities as well. To understand the complete mechanism of these compounds further docking experiments were performed on both TLR-2 (PDB: 2Z80) and TLR-4(PDB: 2Z63), as revealed in (Figures 5 and 6).

As shown in Figure 6 and Table 5, the three active compounds (**4b**, **3a** and **8e**) were found to occupy the same binding site as the reference ligand. For the reference ligand, all non-covalent interactions formed are mostly hydrophilic i.e. COOH and O atom of the ligand interact with Lys B37, Gly B41 and Gln A209, forming Hydrogen bonding with its oxygen. Compound **4b** showed the highest binding affinity to the receptor by forming hydrophobic and hydrophilic interactions (three binding poses). These interactions are as follows: Two hydrophobic interactions with Asp B31 and one hydrogen bonding with Asp A235. Similar to what was shown for COX-2, compound **8e** is still showing the second-best

receptor interactions with two hydrophobic interactions with Lys B37 and Asp B31. Furthermore, compound **3a** showed very good binding affinity with both hydrophobic interactions with Thr A262 and hydrophilic interaction between the —Cl and Asp B106, supporting its good activities in NO-assay (Table 6).

Using TLR-4 as the receptor protein, the reference ligand was found to interact in hydrophilic manner between its oxygen atoms and two amino acid residues (one hydrogen bond each) Glu 89 and Asn 137. Compound **4b** still shows the highest binding affinity with two additional binding interactions more than that of the reference ligand. It interacts with amino acid residues of Asn 137, Glu 89 and forms additional two hydrophobic interactions with Pro 113 amino acid residue. Compound **3a** shows the second best binding affinity with three hydrophobic (aromatic interactions) with Glu 89 and Pro 113 amino acid residues. Finally, compound **8e** forms hydrophilic interactions with both Glu 42 and Glu 89 amino acid residues. These three compounds show the same interaction with Glu 89 as the ligand, and in line with the biological results indicated that the activities of both **3a** and **4b** is greater than **8e** in NO assay. To further understand the activities of the designed compounds, Figure 7 reveals the structure activity relationship (SAR) of the three active compounds.

The docking studies performed concluded that compounds **4b** and **8e** bind tightly to COX-2 and TLR-4 respectively. To further observe the stability of the complex as well as elaborate on the binding energy of interaction, molecular dynamic simulations was conducted for 100ns using GROMACS 2.1.1 software. The MD simulation evaluation was conducted as follows: (1) **RMSD and RMSF analysis:** in the current work, further computational

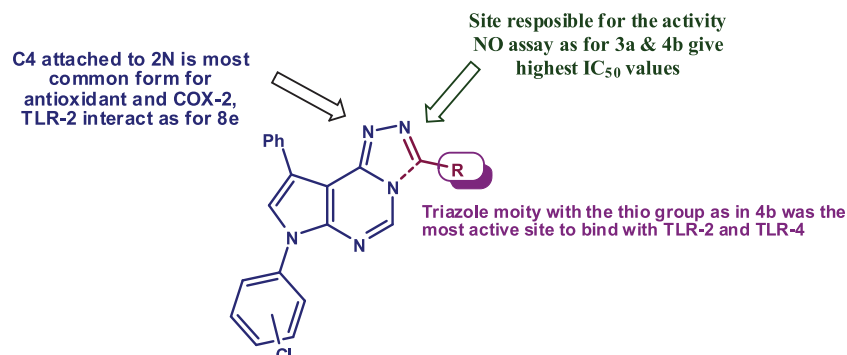


Figure 7. SAR for the active compounds with biological and docking results.

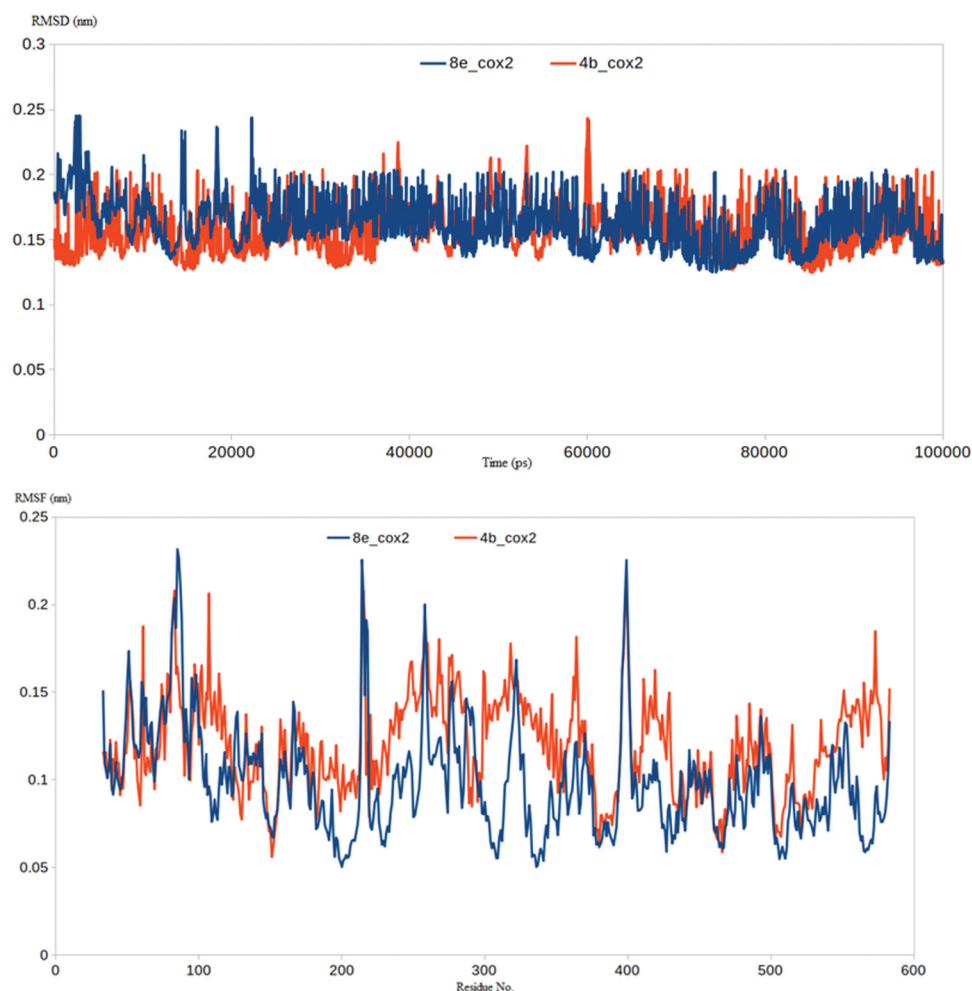


Figure 8. (a) RMSD analysis for the MD simulations of COX2-**4b** and COX2-**8e** complexes; (b) RMSF analysis for the MD simulations of COX2-**4b** and COX2-**8e** complexes.

investigations were achieved through molecular dynamic simulations. Molecular dynamics (MD) simulation provides many valuable information and parameters to study the dynamicity of biological complexes. Amongst this information, MD could provide insights into precise estimation of the binding strength of a docked complex of a ligand and a target. Accordingly, the predicted binding co-ordinates retrieved from the docking of COX-2 and TLR-4 with **4b** and **8e** were moved forward to MD simulation. As demonstrated by Figure 8(a), the two proposed inhibitors had the privilege of forming a stable complex with COX-2 enzyme as indicated by their lower RMSD values. The COX2-**4b** and COX2-**8e**

complexes had RMSD values of 0.2 nm and 0.19 nm, respectively. Similar results were obtained from the RMSF analysis where the residues of COX2-**4b** and COX2-**8e** complexes showed acceptable stabilities with an average RMSF of 0.18 and 0.17 nm, respectively Figure 8(b). The ability of compounds **4b** and **8e** to produce stable complexes as indicated by the low RMSD and RMSF values is a valid indicator on their inhibitory effect on COX-2 enzyme

Similar results were obtained from the molecular simulations of complexes of **4b** and **8e** with TLR-4. The TLR-4-**4b** and TLR-4-**8e** complexes had RMSD values of 0.18 nm and 0.22 nm, respectively Figure 9(a). Besides, most of the residues of TLR-4-**4b** and TLR-4-

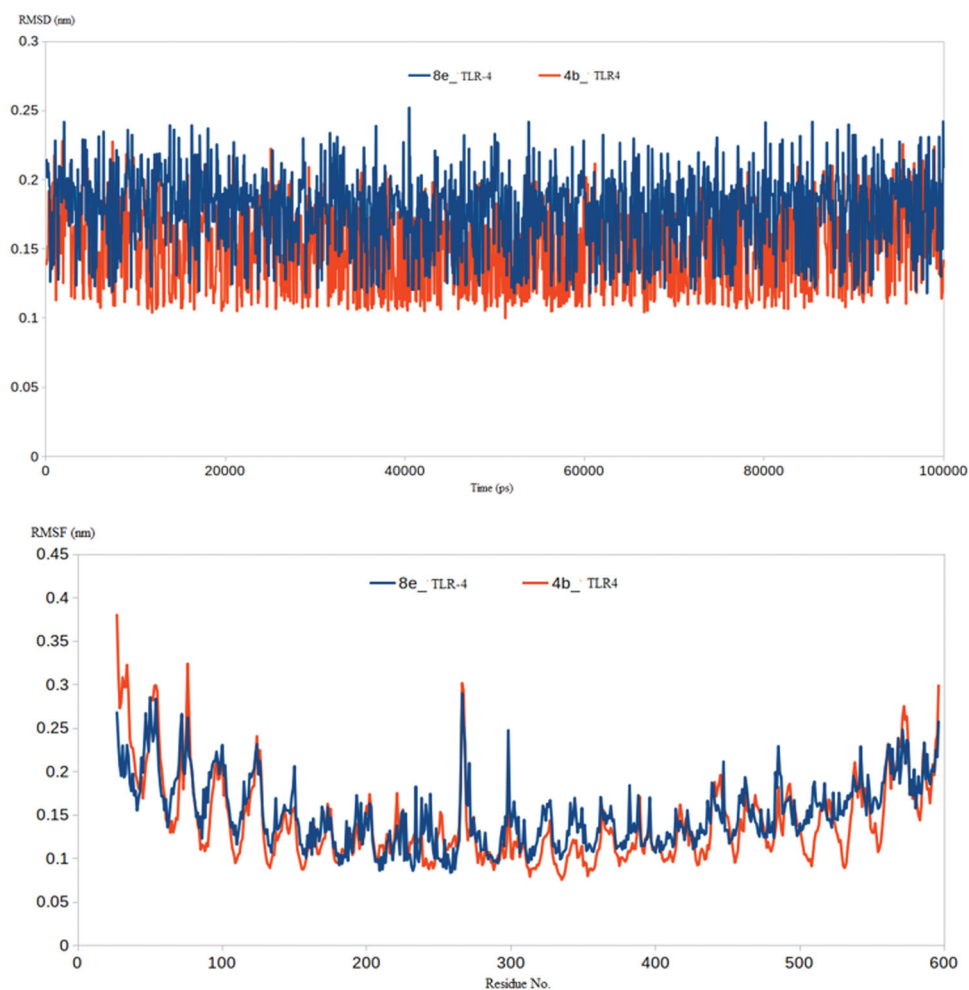


Figure 9. (a) RMSD analysis for the MD simulations of TLR-4**4b** and TLR-4**8e** complexes; (b) RMSF analysis for the MD simulations of TLR-4**4b** and TLR-4**8e** complexes.

Table 7. The binding free energies of **4b** and **8e** in complex with COX-2 and TLR-4.

Complex	$\Delta E_{\text{binding}}$ (kJ/mol)	$\Delta E_{\text{Electrostatic}}$ (kJ/mol)	$\Delta E_{\text{Vander Waal}}$ (kJ/mol)	$\Delta E_{\text{polar solvation}}$ (kJ/mol)	SASA (kJ/mol)
4b -COX-2	-87 ± 2.3	-57.1 ± 2.2	-73.1 ± 2.3	56.9 ± 1.3	-13.7 ± 0.1
8e -COX-2	-89.1 ± 2.0	-62.5 ± 1.9	-69.9 ± 2.0	55.8 ± 1.2	-12.5 ± 0.2
4b -TLR-4	-106.2 ± 1.8	-65.6 ± 1.8	-77.7 ± 1.9	54.4 ± 1.5	-17.3 ± 0.2
8e -TLR-4	-81.9 ± 1.5	-55.1 ± 1.5	-59.7 ± 1.6	48.7 ± 1.4	-15.8 ± 0.1

8e complexes reached an average RMSF of 0.19 and 0.21 nm, respectively [Figure 9\(b\)](#). In conclusion, the RMSD and RMSF analysis of the formed complexes between **4b** and **8e** with COX-2 and TLR-4 showed favourable stability for both the compounds and emphasised the results from the experimental assays. (2) **Binding Free Energy Calculations using MM-PBSA approach:** attempting to further endorse the binding strength between the COX-2 enzyme and TLR-4 with the newly developed compounds **4b** and **8e**, the *g_mmpbsa* package was brought in action to compute the binding free energies between the two targets and the proposed molecules **4b** and **8e**. The generated trajectories from the production stage were used to calculate all the forms of binding free energy. These energy types include electrostatic energy, van der Waal energy, polar solvation energy and SASA energy. All the previous types of energy were calculated for the four complexes containing COX-2 and TLR-4 bound to **4b** or **8e** ([Table 7](#)).

Interestingly as shown in [Table 7](#), the calculated binding free energy for the two small molecules were favourable in which

compound **4b** achieved binding free energies of -87 ± 2.3 and -106.2 ± 1.8 (kJ/mol) with COX-2 and TLR-4, respectively. On the other hand, compound **8e** achieved binding free energies of -89.1 ± 2.0 and -81.9 ± 1.5 (kJ/mol) with COX-2 and TLR-4, respectively. These results augmented all the *in-silico* calculations giving credit to the predicted binding mode of both **4b** and **8e** within COX-2 and TLR-4 binding sites.

Conclusions

In this study, we have presented the design, synthesis and biological evaluation of novel arylidineaminopyrrolopyrimidine, and their fused form triazolo-pyrrolopyrimidine, that can act as antioxidant and anti-inflammatory promising agents utilising LPS-induced macrophages (RAW264.7) cells. The present study report that pyrrolopyrimidines (**3a**, **4b** and **8e**) manage to fit in new Toll 2 and 4 receptors in exceptionally great manners supported by molecular modelling and simulations compared to well-known ligand. In

addition, we reported their mechanism action as anti-COX2 agents, as conceivable proposed novel pathway for their anti-inflammatory aside with anti-oxidant activities.

Disclosure statement

No potential conflict of interest was reported by the author(s).

Funding

The author(s) reported there is no funding associated with the work featured in this article.

References

1. Yu L, Feng Z. The role of toll-like receptor signaling in the progression of heart failure. *Mediators Inflamm* 2018;2018: 9874109.
2. Zhang Y, Liang C. Innate recognition of microbial-derived signals in immunity and inflammation. *Sci China Life Sci* 2016;59:1210–7.
3. Wong SW, Kwon MJ, Choi AMK, et al. Fatty acids modulate toll-like receptor 4 activation through regulation of receptor dimerization and recruitment into lipid rafts in a reactive oxygen species-dependent manner. *J Biol Chem* 2009; 284:27384–92.
4. Wang Y, Song E, Bai B, Vanhoutte PM. Toll-like receptors mediating vascular malfunction: lessons from receptor subtypes. *Pharmacol Ther* 2016;158:91–100.
5. Momtazmanesh S, Perry G, Rezaei N. Toll-like receptors in Alzheimer's disease. *J Neuroimmunol* 2020;348:577362.
6. Jialal I, Kaur H, Devaraj S. Toll-like receptor status in obesity and metabolic syndrome: a translational perspective. *J Clin Endocrinol Metab* 2014;99:39–48.
7. Farrugia M, Baron B. The role of toll-like receptors in autoimmune diseases through failure of the self-recognition mechanism. *Int J Inflam* 2017;2017:8391230.
8. Azam S, Jakaria M, Kim IS, et al. Regulation of toll-like receptor (TLR) signaling pathway by polyphenols in the treatment of age-linked neurodegenerative diseases: focus on TLR4 signaling. *Front Immunol* 2019;10:1000.
9. Huang Q-Q, Pope RM. The role of toll-like receptors in rheumatoid arthritis. *Curr Rheumatol Rep* 2009;11:357–64.
10. So EY, Ouchi T. The application of toll like receptors for cancer therapy. *Int J Biol Sci* 2010;6:675–81.
11. Tsujimoto H, Ono S, Efron PA, et al. Role of toll-like receptors in the development of sepsis. *Shock* 2008;29:315–21.
12. Li Y, Deng S-L, Lian Z-X, Yu K. Roles of toll-like receptors in nitroxidative stress in mammals. *Cells* 2019;8:576.
13. Yang L, Xie X, Tu Z, et al. The signal pathways and treatment of cytokine storm in COVID-19. *Signal Transduct Target Ther* 2021;6:1–20.
14. Masih A, Agnihotri AK, Srivastava JK, et al. Discovery of novel pyrazole derivatives as a potent anti-inflammatory agent in RAW264.7 cells via inhibition of NF- κ B for possible benefit against SARS-CoV-2. *J Biochem Mol Toxicol* 2021; 35:1–9.
15. Kim JS, Lee JY, Yang JW, et al. Immunopathogenesis and treatment of cytokine storm in COVID-19. *Theranostics* 2021;11:316–29.
16. Berrios-Cárcamo P, Quezada M, Quintanilla ME, et al. Oxidative stress and neuroinflammation as a pivot in drug abuse. A focus on the therapeutic potential of antioxidant and anti-inflammatory agents and biomolecules. *Antioxidants* 2020;9:830–26.
17. Gay NJ, Symmons MF, Gangloff M, Bryant CE. Assembly and localization of toll-like receptor signalling complexes. *Nat Rev Immunol* 2014;14:546–58.
18. Sellge G, Kufer TA. PRR-signaling pathways: learning from microbial tactics. *Semin Immunol* 2015;27:75–84.
19. Mukherjee S, Karmakar S, Babu SPS. TLR2 and TLR4 mediated host immune responses in major infectious diseases: a review. *Brazilian J Infect Dis* 2016;20:193–204.
20. Pudney J, X H, Z M, et al. Differential expression of toll-like receptors in the human placenta across early gestation. *Placenta* 2016;46:1–10.
21. Delneste Y, Beauvillain C, Jeannin P. Innate immunity: structure and function of TLRs. *Medicine/Sciences* 2007;23: 67–73.
22. El-Zayat SR, Sibaii H, Mannaa FA. Toll-like receptors activation, signaling, and targeting: an overview. *Bull Natl Res Cent* 2019;43:187.
23. Medzhitov R, Preston-Hurlburt P, Janeway CA. A human homologue of the *Drosophila* toll protein signals activation of adaptive immunity. *Nature* 1997;388:394–7.
24. Lee CC, Avalos AM, Ploegh HL. Accessory molecules for Toll-like receptors and their function. *Nat Rev Immunol* 2012;12:168–79.
25. Molinaro A, Holst O, Lorenzo FD, et al. Chemistry of lipid A: at the heart of innate immunity. *Chem - A Eur J* 2015;21: 500–19.
26. O'Neill LAJ, Golenbock D, Bowie AG. The history of Toll-like receptors-redefining innate immunity. *Nat Rev Immunol* 2013;13:453–60.
27. Park S, Shin H-J, Shah M, et al. TLR4/MD2 specific peptides stalled in vivo LPS-induced immune exacerbation. *Biomaterials* 2017;126:49–60.
28. Firmal P, Shah VK, Chattopadhyay S. Insight into TLR4-mediated immunomodulation in normal pregnancy and related disorders. *Front Immunol* 2020;11:807–16.
29. Ciesielska A, Matyjek M, Kwiatkowska K. TLR4 and CD14 trafficking and its influence on LPS-induced pro-inflammatory signaling. *Cell Mol Life Sci* 2021;78:1233–61.
30. Yong-Bing X, Gui-Lin C, Ming-Quan G. Antioxidant and anti-inflammatory activities of the crude extracts of *Moringa oleifera* from Kenya and their correlations with flavonoids. *Antioxidants* 2019;8:296.
31. Battilocchio C, Poce G, Alfonso S, et al. A class of pyrrole derivatives endowed with analgesic/anti-inflammatory activity. *Bioorganic Med Chem* 2013;21:3695–701.
32. Kuzmich NN, Sivak KV, Chubarev VN, et al. TLR4 signaling pathway modulators as potential therapeutics in inflammation and sepsis. *Vaccines* 2017;5:34–25.
33. Mohame MS, Mostafa AG, El-hameed RHA, et al. Evaluation of the anti-inflammatory activity of novel synthesized pyrrole, pyrrolopyrimidine and spiropyrrolopyrimidine derivatives. *Pharmacophore* 2012;3:44–54.
34. Mohamed MS, Kamel R, Fatahala SS. Synthesis and biological evaluation of some thio containing pyrrolo [2, 3-d] pyrimidine derivatives for their anti-inflammatory and antimicrobial activities. *Eur J Med Chem* 2010;45:2994–3004.
35. Mohamed MS, Kamel R, Fathallah SS. Synthesis of new pyrroles of potential anti-inflammatory activity. *Arch Pharm* 2011;344:830–9.

36. Mohamed MS, Awad SM, Sayed AI. Synthesis of certain pyrimidine derivatives as antimicrobial agents and anti-inflammatory agents. *Molecules* **2010**;15:1882–90.
37. Mohamed MS, Abd-El Hameed RH, Sayed AI, Soror SH. Novel antiviral compounds against gastroenteric viral infections. *Arch Pharm* **2015**;348:194–205.
38. Mohamed MS, Sayed AI, Khedr MA, et al. Evaluation of novel pyrrolopyrimidine derivatives as antiviral against gastroenteric viral infections. *Eur J Pharm Sci* **2019**;127:102–14.
39. Zander U, Hoffmann G, Cornaciu I, et al. Automated harvesting and processing of protein crystals through laser photobleaching research papers. *Acta Cryst* **2016**;72:454–66.
40. Jin MS, Kim SE, Heo JY, et al. Crystal structure of the TLR1-TLR2 heterodimer induced by binding of a tri-acylated lipopeptide. *Cell* **2007**;130:1071–82.
41. Friedman JM, Lee GH, Proenca R, et al. Abnormal splicing of the leptin receptor in diabetic mice. *Nature* **1996**;379:632–5.
42. Kim HM, Park BS, Kim JI, et al. Crystal structure of the TLR4-MD-2 complex with bound endotoxin antagonist eritoran. *Cell* **2007**;130:906–17.
43. Abraham MJ, Murtola T, Schulz R, et al. Gromacs: high performance molecular simulations through multi-level parallelism from laptops to supercomputers. *SoftwareX* **2015**;1:2:19–25.
44. Schüttelkopf AW, Van Aalten DMF. PRODRG: a tool for high-throughput crystallography of protein-ligand complexes. *Acta Crystallogr Sect D Biol Crystallogr* **2004**;60:1355–63.
45. El Hassab MA, Eldehna WM, Al-Rashood ST, et al. Multi-stage structure-based virtual screening approach towards identification of potential SARS-CoV-2 NSP13 helicase inhibitors. *J Enzyme Inhib Med Chem* **2022**;37:563–72.
46. Kumari R, Kumar R, Lynn A. g_mmpbsa—a GROMACS tool for high-throughput MM-PBSA calculations. *J Chem Inf Model* **2014**;54:1951–62.
47. BLOIS MS. Antioxidant determinations by the use of a stable free radical. *Nature* **1958**;181:1199–200.
48. Solaiman MA, Ali MA, Abdel-Moein NM, Mahmoud EA. Synthesis of Ag-NPs developed by green-chemically method and evaluation of antioxidant activities and anti-inflammatory of synthesized nanoparticles against LPS-induced NO in RAW 264.7 macrophages. *Biocatal Agric Biotechnol* **2020**;29:101832.
49. Khor KZ, Joseph J, Shamsuddin F, et al. The cytotoxic effects of *Moringa oleifera* leaf extract and silver nanoparticles on human kasumi-1 cells. *Int J Nanomedicine* **2020**;15:5661–70.
50. Vishwakarma A, Wany A, Pandey S, et al. Current approaches to measure nitric oxide in plants. *J Exp Bot* **2019**;70:4333–43.
51. Zaki RM, El Dean AMK, El Monem MIA, Seddik MA. Novel synthesis and reactions of pyrazolyl-substituted tetrahydrothieno[2,3-c]isoquinoline derivatives. *Heterocycl Commun* **2016**;22:103–9.
52. Hossain MI, Bhuiyan MMH. Synthesis and antimicrobial activities of some new thieno and furopyrimidine derivatives. *J Sci Res* **2009**;1:317–25.
53. Flefel EM, El-Sofany WI, El-Shahat M, et al. Synthesis, molecular docking and in vitro screening of some newly synthesized triazolopyridine, pyridotriazine and pyridine-pyrazole hybrid derivatives. *Molecules* **2018**;23:2548.
54. Mohamed MS, Kamel R, Abd El-Hameed RH. Evaluation of the anti-inflammatory activity of some pyrrolo[2,3-d] pyrimidine derivatives. *Med Chem Res* **2013**;22:2244–52.
55. Fatahala SS, Khedr MA, Mohamed MS. Synthesis and structure activity relationship of some indole derivatives as potential anti-inflammatory agents. *Acta Chim Slov* **2017**;64:865–76.
56. Fatahala SSSS, Hasabelnaby S, Goudah A, et al. Pyrrole and fused pyrrole compounds with bioactivity against inflammatory mediators. *Molecules* **2017**;22:461–18.
57. Ghoshal T, Patel TM. Anticancer activity of benzoxazole derivative (2015 onwards): a review. *Futur J Pharm Sci* **2020**;6:94.
58. Abdel-Mohsen SA. Synthesis, reactions and antimicrobial activity of 2-amino-4-(8-quinolinol-5-yl)-1-(p-tolyl)-pyrrole-3-carbonitrile. *Bull Korean Chem Soc* **2005**;26:719–28.
59. Yehye WA, Abdul N, Arif A, et al. Understanding the chemistry behind the antioxidant activities of butylated hydroxytoluene (BHT): a review. *Eur J Med Chem* **2015**;101:295–310.
60. Hsu FL, Huang WJ, Wu TH, et al. Evaluation of antioxidant and free radical scavenging capacities of polyphenolics from pods of *Caesalpinia pulcherrima*. *Int J Mol Sci* **2012**;13:6073–88.
61. Debnath U, Mukherjee S, Joardar N, et al. Aryl quinolinyl hydrazone derivatives as anti-inflammatory agents that inhibit TLR4 activation in the macrophages. *Eur J Pharm Sci* **2019**;134:102–15.
62. Almasaudi SB, El-Shitany NA, Abbas AT, et al. Antioxidant, anti-inflammatory, and antiulcer potential of manuka honey against gastric ulcer in rats. *Oxid Med Cell Longev* **2016**;2016:3643824–10.
63. Klementiev B, Li S, Korshunova I, et al. Anti-inflammatory properties of a novel peptide interleukin 1 receptor antagonist. *J Neuroinflammation* **2014**;11:27.
64. ElBordiny HS, El-Miligy MM, Kassab SE, et al. Design, synthesis, biological evaluation and docking studies of new 3-(4,5-dihydro-1H-pyrazol-5-yl)-2-phenyl-1H-indole derivatives as potent antioxidants and 15-lipoxygenase inhibitors. *Eur J Med Chem* **2018**;145:594–605.
65. Amorim JL, Simas DLR, Pinheiro MMG, et al. Anti-inflammatory properties and chemical characterization of the essential oils of four *Citrus* species. *PLoS One* **2016**;11:e0153643–18.
66. Toledo TR, Dejana NN, Monnazzi LGS, et al. Potent anti-inflammatory activity of pyrenocine A isolated from the marine-derived fungus *Penicillium paxilli* Ma(G)K. *Mediators Inflamm* **2014**;2014:767061.
67. Jose SP, M R, S S, et al. Anti-inflammatory effect of Kaba Sura Kudineer (AYUSH approved COVID-19 drug)-a Siddha poly-herbal formulation against lipopolysaccharide induced inflammatory response in RAW-264.7 macrophages cells. *J Ethnopharmacol* **2022**;283:114738.
68. Forcados GE, Muhammad A, Oladipo OO, et al. Metabolic implications of oxidative stress and inflammatory process in SARS-CoV-2 pathogenesis: therapeutic potential of natural antioxidants. *Front Cell Infect Microbiol* **2021**;11:654813–1.
69. Saeedi-Boroujeni A, Mahmoudian-Sani MR. Anti-inflammatory potential of quercetin in COVID-19 treatment. *J Inflamm* **2021**;18:1–9.
70. Rashid H. u, Martines MAU, Duarte AP, et al. Research developments in the syntheses, anti-inflammatory activities

- and structure-activity relationships of pyrimidines. *RSC Adv* **2021**;11:6060–98.
71. Saleh HA, Yousef MH, Abdelnaser A. The anti-inflammatory properties of phytochemicals and their effects on epigenetic mechanisms involved in TLR4/NF- κ B-mediated inflammation. *Front Immunol* **2021**;12:606069–29.
 72. Menche D. Design and synthesis of simplified polyketide analogs: new modalities beyond the rule of 5. *ChemMedChem* **2021**;16:2068–74.
 73. Wu J, Liu B, Mao W, et al. Prostaglandin E2 regulates activation of mouse peritoneal macrophages by *Staphylococcus aureus* through toll-like receptor 2, toll-like receptor 4, and NLRP3 inflammasome signaling. *J Innate Immun* **2020**;12:154–69.
 74. Ren H, Chen X, Jiang F, Li G. Cyclooxygenase-2 inhibition reduces autophagy of macrophages enhancing extraintestinal pathogenic *Escherichia coli* infection. *Front Microbiol* **2020**;11:708–10.
 75. Ono Y, Maejima Y, Saito M, et al. TAK-242, a specific inhibitor of Toll-like receptor 4 signalling, prevents endotoxemia-induced skeletal muscle wasting in mice. *Sci Rep* **2020**;10:1–13.
 76. Abdulkareem Aljumaily SA, Demir M, Elbe H, et al. Antioxidant, anti-inflammatory, and anti-apoptotic effects of crocin against doxorubicin-induced myocardial toxicity in rats. *Environ Sci Pollut Res* **2021**;28:65802–13.
 77. Makbal R, Idrissi FEJ, Ouchbani T, et al. Anti-inflammatory, antioxidant, chemical characterization, and safety assessment of *Argania spinosa* fruit shell extract from South-Western Morocco. *Biomed Res Int* **2021**;2021:5536030.
 78. Chen CJ, Liu YP. Merit inhibition: potential as a treatment strategy in EGFR tyrosine kinase inhibitor-resistant non-small cell lung cancer. *Pharmaceuticals* **2021**;14:130–25.
 79. Ha MW, Paek SM. Recent advances in the synthesis of ibuprofen and naproxen. *Molecules* **2021**;26:4792.
 80. Santos-Sierra S. Targeting Toll-like receptor (TLR) pathways in inflammatory arthritis: two better than one? *Biomolecules* **2021**;11:1291.
 81. Chen L, Ji X, Wang M, et al. Involvement of TLR4 signaling regulated-COX2/PGE2 axis in liver fibrosis induced by *Schistosoma japonicum* infection. *Parasites Vectors* **2021**;14:1–13.
 82. Algehani RA, Abou R, Hegazy GA, et al. Colosolactone-G synergizes the anticancer properties of 5-fluorouracil and gemcitabine against colorectal cancer cells. *Biomed Pharmacother* **2021**;140:111730.
 83. ul Ain Q, Batool M, Choi S. TLR4-targeting therapeutics: structural basis and computer-aided drug discovery approaches. *Molecules* **2020**;25:627.
 84. Di Lorenzo A, Bolli E, Tarone L, et al. Toll-like receptor 2 at the crossroad between cancer cells, the immune system, and the microbiota. *Int J Mol Sci* **2020**;21:9418–26.
 85. Alizadeh M, Jalal M, Hamed K, et al. Recent updates on anti-inflammatory and antimicrobial effects of furan natural derivatives. *J Inflamm Res* **2020**;13:451–63.
 86. Cao H, Sethumadhavan K. Regulation of cell viability and anti-inflammatory tristetraprolin family gene expression in mouse macrophages by cottonseed extracts. *Sci Rep* **2020**;10:1–11.
 87. Wang Y, Zhang S, Li H, et al. Small-molecule modulators of Toll-like receptors. *Acc Chem Res* **2020**;53:1046–55.
 88. Nie X, Kitaoka S, Shinohara M, et al. Roles of Toll-like receptor 2/4, monoacylglycerol lipase, and cyclooxygenase in social defeat stress-induced prostaglandin E2 synthesis in the brain and their behavioral relevance. *Sci Rep* **2019**;9:1–10.
 89. Facchini FA, Zaffaroni L, Minotti A, et al. Structure-activity relationship in monosaccharide-based toll-like receptor 4 (TLR4) antagonists. *J Med Chem* **2018**;61:2895–909.
 90. Zaffaroni L, Peri F. Recent advances on Toll-like receptor 4 modulation: new therapeutic perspectives. *Future Med Chem* **2018**;10:461–76.
 91. Wang W, Wang J. Toll-like receptor 4 (TLR4)/cyclooxygenase-2 (COX-2) regulates prostate cancer cell proliferation, migration, and invasion by NF- κ B activation. *Med Sci Monit* **2018**;24:5588–97.
 92. Wang X, Yao B, Wang Y, et al. Macrophage cyclooxygenase-2 protects against development of diabetic nephropathy. *Diabetes* **2017**;66:494–504.
 93. Lin A, Wang G, Zhao H, et al. TLR4 signaling promotes a COX-2/PGE2/STAT3 positive feedback loop in hepatocellular carcinoma (HCC) cells. *Oncoimmunology* **2016**;5:e1074376–11.
 94. Marshall JD, Heeke DS, Rao E, et al. A novel class of small molecule agonists with preference for human over mouse TLR4 activation. *PLoS One* **2016**;11:e0164632–30.
 95. Elisha IL, Dzoyem JP, McGaw LJ, et al. The anti-arthritis, anti-inflammatory, antioxidant activity and relationships with total phenolics and total flavonoids of nine South African plants used traditionally to treat arthritis. *BMC Complement Altern Med* **2016**;16:1–10.
 96. Makene VW, Pool EJ. The assessment of inflammatory activity and toxicity of treated sewage using RAW264.7 cells. *Water Environ J* **2015**;29:353–9.
 97. Chen CY, Kao CL, Liu CM. The cancer prevention, anti-inflammatory and anti-oxidation of bioactive phytochemicals targeting the TLR4 signaling pathway. *Int J Mol Sci* **2018**;19:2729.
 98. Zhao Y, Yang Y, Liu M, et al. COX-2 is required to mediate crosstalk of ROS- dependent activation of MAPK/NF- κ B signaling with pro-inflammatory response and defense-related NO enhancement during challenge of macrophage-like cell line with *Giardia duodenalis*. *PLoS Negl Trop Dis* **2022**;16:e0010402.
 99. Jannus F, Medina-o'donnell M, Neubrand VE, et al. Efficient in vitro and in vivo anti-inflammatory activity of a diamine-pegylated oleanolic acid derivative. *Int J Mol Sci* **2021**;22:8158.
 100. Abd El-Hameed RH, Mahgoub S, El-Shanbaky HM, Mohamed MS, et al. Utility of novel 2-furanones in synthesis of other heterocyclic compounds having anti-inflammatory activity with dual COX2/LOX inhibition. *J Enzyme Inhib Med Chem* **2021**;36:977–86.
 101. Shen C, Liu H, Wang X, et al. Importance of incorporating protein flexibility in molecule modeling: a theoretical study on type I1/2 NIK inhibitors. *Front Pharmacol* **2019**;10:345.
 102. Hwang JH, Ma JN, Park JH, et al. Anti-inflammatory and antioxidant effects of MOK, a polyherbal extract, on lipopolysaccharide-stimulated RAW 264.7 macrophages. *Int J Mol Med* **2019**;43:26–36.
 103. Chen L, Zhang JP, Liu X, et al. Semisynthesis, an anti-inflammatory effect of derivatives of 1 β -hydroxy alantolactone from *Inula britannica*. *Molecules* **2017**;22:1835–8.
 104. Lv H, Liu Q, Wen Z, et al. Xanthohumol ameliorates lipopolysaccharide (LPS)-induced acute lung injury via induction of AMPK/GSK3 β -Nrf2 signal axis. *Redox Biol* **2017**;12:311–24.

105. Banerjee AG, Das N, Shengule SA, et al. Synthesis, characterization, evaluation and molecular dynamics studies of 5, 6-diphenyl-1,2,4-triazin-3(2H)-one derivatives bearing 5-substituted 1,3,4-oxadiazole as potential anti-inflammatory and analgesic agents. *Eur J Med Chem* **2015**;101:81–95.
106. Bergandi L, Apprato G, Silvagno F. Antioxidant and anti-inflammatory activity of combined phycocyanin and palmitoylethanolamide in human lung and prostate epithelial cells. *Antioxidants* **2022**;11:201.
107. Vien LT, Hanh TTH, Huong PTT, et al. Pyrrole oligoglycosides from the starfish *Acanthaster planci* suppress lipopolysaccharide-induced nitric oxide production in RAW264.7 macrophages. *Chem Pharm Bull* **2016**;64:1654–7.
108. Mateev E, Georgieva M, Zlatkov A. Pyrrole as an important scaffold of anticancer drugs: recent advances. *J Pharm Pharm Sci* **2022**;25:24–40.
109. Bindu S, Mazumder S, Bandyopadhyay U. Non-steroidal anti-inflammatory drugs (NSAIDs) and organ damage: a current perspective. *Biochem Pharmacol* **2020**;180:114147.
110. Jeelan Basha N, Basavarajaiah SM, Shyamsunder K. Therapeutic potential of pyrrole and pyrrolidine analogs: an update. *Mol Divers* **2022**;1–23.
111. Lattuca B, Khoueiry Z, Malclès G, et al. Drug interactions between non-steroidal anti-inflammatory drugs and cardiovascular treatments (except anti-agregant therapy). *Antiinflamm Antiallergy Agents Med Chem* **2013**;12:36–46.
112. Ushiyama S, Yamada T, Murakami Y, et al. Preclinical pharmacology profile of CS-706, a novel cyclooxygenase-2 selective inhibitor, with potent antinociceptive and anti-inflammatory effects. *Eur J Pharmacol* **2008**;578:76–86.
113. Howes LG. Selective COX-2 inhibitors, NSAIDs and cardiovascular events – is celecoxib the safest choice? *Ther Clin Risk Manag* **2007**;3:831–45.
114. Bocheva A, Bijev A, Nankov A. Further evaluation of a series of anti-inflammatory N-pyrrolylcarboxylic acids: effects on the nociception in rats. *Arch Pharm* **2006**;339:141–4.
115. Lessigiarska I, Nankov A, Bocheva A, et al. 3D-QSAR and preliminary evaluation of anti-inflammatory activity of series of N-pyrrolylcarboxylic acids. *Farmaco* **2005**;60:209–18.